1.94 Å structure of synthetic α-synuclein fibrils seeding MSA neuropathology

Domenic Burger, Marianna Kashyrina, Amanda J Lewis, Francesco de Nuccio, Inayathulla Mohammed, Hortense de la Seiglière, Lukas van den Heuvel, Jérémy Verchère, Cécile Feuillie, Mélanie Berbon, et al.

1.94 Å structure of synthetic α-synuclein fibrils seeding MSA neuropathology

Domenic Burger[1,2], Marianna Kashyrina[3,4], Amanda J. Lewis[1,2], Francesco De Nuccio[4], Inayathulla Mohammed[1,2,5], Hortense de La Seiglière[3], Lukas van den Heuvel[1,2], Jérémy Verchère[6], Cécile Feuillie[7], Mélanie Berbon[7], Marie-Laure Arotçarena[3], Aude Retailleau[3], Erwan Bezard[3], Florent Laferrière[3], Antoine Loquet[7], Luc Bousset[8], Thierry Baron[6], Dario Domenico Lofrumento[4], Francesca De Giorgi[3], Henning Stahlberg[1,2,#], and François Ichas[3,4,#].

1. Laboratory of Biological Electron Microscopy, Institute of Physics, School of Basic Science, EPFL Lausanne, Switzerland
2. Department of Fundamental Microbiology, Faculty of Biology and Medicine, UNIL, Route de la Sorge, 1015 Lausanne, Switzerland
3. Univ. Bordeaux, CNRS, IMN, UMR 5293, F-33000 Bordeaux, France
4. Univ. Salento, DiSTeBA, Human Anatomy, I-73100 Lecce, Italy
5. Dubochet Center for Imaging, Lausanne, Genopode (UNIL), EPFL, 1015 Lausanne, Switzerland
6. Univ. Lyon, ANSES, Neurodegenerative Diseases Unit, F-69364 Lyon, France
7. Univ. Bordeaux, CNRS, CBMN, UMR 5248, F-33600 Pessac, France
8. Univ. Paris-Saclay, CNRS, CEA, LMN, UMR 9199, F-92265 Fontenay-aux-Roses, France

Correspondence to: henning.stahlberg@epfl.ch and francois.ichas@inserm.fr

Abstract

Multiple system atrophy (MSA) is a rapidly progressive neurodegenerative disease of unknown etiology, typically affecting individuals aged 50-60 and leading to patient death within a decade[1–3]. Characterized by the presence of oligodendroglial intracellular aggregates (GCIs) primarily composed of fibrillar alpha-synuclein (aSyn)[4–8], formation of MSA neuropathology presents similarities to prion propagation[9,10]. While previous investigations have scrutinized fibrils extracted from MSA brains[11], their "protein-only" replication was questioned[12] and their capacity to induce GCIs in animal models was not explored. Conversely, the synthetic fibril strain 1B[13,14] assembled from recombinant human aSyn self-replicates autonomously *in vitro* and induces GCIs in mice[15], suggesting relevance to MSA. Here we report the high-resolution structural analysis of the 1B fibrils revealing similarities with human brain extracted MSA aSyn filaments, particularly the lack of a specific Thioflavin T (ThT) binding pocket[16]. In addition, 1B causes sustained intracerebral GCI spread over the years, prompt lethality in transgenic mice, and transmission of inclusion pathology to wild-type animals after crude brain homogenate inoculation. This points to an underlying prion-like seeding process which we demonstrate *in situ* using correlative light-electron microscopy. Our findings underscore structural features of aSyn fibrils pivotal for MSA pathogenesis and provide insights for therapeutic development.

Main

Multiple system atrophy (MSA) is characterized by the rapid invasion of the brainstem, the cerebellum and/or the basal ganglia by intracellular inclusions filled with fibrillar alpha-synuclein[4–8]. These inclusions appear in neurons and in oligodendrocytes (OLs), particularly within the myelinated bundles of the white matter[17–19]. The latter inclusions are called glial cytoplasmic inclusions (GCIs) and are specific to MSA. They are only observed rarely in other sporadic alpha-synucleinopathies[2,3]. The phenomenon of a "step-by-step" progression that characterizes brain invasion by GCIs, and the speed at which the GCIs induce the death of neurons in myelinated tracts[3], has led to the notion that MSA may obey a molecular mechanism analogous to that governing the intracerebral diffusion of pathogenic prions[9,10]. According to this hypothesis, the specific alpha-synuclein fibril strain found in GCIs plays a central role as both initiator and propagator of the pathology[9,10].

Alpha-synuclein (aSyn) fibrils in GCIs were first observed *in situ*[4–8], and extracted and described using electron microscopy more than 25 years ago[20,21]. Such fibrils, extracted using the detergent sarkosyl, were characterized at high resolution by cryo-transmission electron microscopy (cryo-EM)[11], but to date, it has not been demonstrated that they can self-replicate like prions or induce the formation of GCIs in animal models. The hypothesis was put forward[12] that unknown cofactors might be required for the replication of these extracted assemblies.

In parallel to the extractive approach by Schweighauser et al.[11], three synthetic aSyn fibril strains were obtained from recombinant aSyn, and these fibrils could self-replicate *in vitro* without the need for an external cofactor, and induce GCIs in mice. Chronologically, the first strain was a non-helical double-filament fibrillar assembly (ribbons) composed of monomers of human aSyn, which were capable of inducing GCIs, but only in mice overexpressing human aSyn concomitantly[22]. The second strain corresponded to mouse synthetic aSyn fibrils, which could induce the delayed appearance of GCIs in non-transgenic mice[23]. Finally, the third case concerned a fibril strain that some of us isolated and characterized (strain 1B), formed this time of human recombinant aSyn, and capable of causing the rapid appearance of GCIs in interfascicular OLs of wild-type mice[15]. Unlike for the aSyn fibrils extracted from MSA patients, no high-resolution atomic structure of these three types of synthetic aSyn fibrils had so far been available. This prevented the comparison of these fibrils with the atomic models obtained from patients to understand the structural bases of their capacity to induce GCIs.

As indirect structural characterization, however, it is interesting to note that not only are all three strains of synthetic aSyn fibrils capable of inducing the formation of GCIs *in vivo*, but they also all show a very low detectability by Thioflavin T (ThT), which is used to routinely detect the vast majority of amyloid-like fibrils[14,24,25]. This suggests that all three aSyn fibril strains share a configuration that is somehow “closed” towards ThT at their outer fibril surfaces, in regions that are typically involved in ThT binding in other aSyn fibril strains. However, those other ThT-positive strains are incapable of inducing GCIs *in vivo*. The observation of aSyn fibrils showing "invisibility" to ThT is remarkable, as it had been reported that seeded aSyn fibril amplification assays using brain samples of MSA patients also resulted in the appearance of ThT-negative aggregates, while amplification with brain samples from Parkinson's disease (PD) patients produced ThT-positive aggregates[26].

The recent high-resolution structural characterization of the ThT binding sites[16] on Type 1a aSyn fibrils[27] which are ThT-positive[28] and which were never reported to induce GCIs, allows us to hypothesize that the loss of one or more of these ThT binding sites might correlate with the appearance of specific biological properties, in particular the ability to seed GCIs.

We here report the structural characterization of aSyn fibrils of strain 1B at a resolution of 1.94 Å, compare them to aSyn filaments extracted from the brains of deceased MSA patients, show their spreading capacity *in vivo* in wild-type and transgenic mice, as well as in primary neuronal cell cultures expressing several aSyn mutants showing distinct propensities towards propagation. We also demonstrate intracellular fibril seeding by 1B *in vivo* using correlative light-electron microscopy (CLEM) supporting an underlying prion-like mechanism for the formation of neuropathology.

Neuropathology seeded in vivo by the synthetic fibril strain 1B

1B fibrils are "ThT-negative" fibrils which we first found capable to elicit a particularly strong aSyn pathology in mice made of Lewy neurites and neuronal cytoplasmic inclusions (NCIs), and most strikingly, of neuronal intranuclear inclusions (NIIs)[13,14]. This attracted our attention because NIIs are distinctive for MSA compared to PD or dementia with Lewy bodies (DLB)[29–31] in which NIIs are absent. Strikingly, the same year, the group of Soto published that fibrils amplified *in vitro* using brain or cerebro-spinal fluid (CSF) samples from MSA patients as templates were also "ThT-negative" compared to amplifications using PD patient templates[26].

This led us to investigate the possibility that the synthetic 1B fibrils could represent an MSA-like fibril strain. Using a directed anatomical approach, we indeed observed that 6 months after intracerebral inoculation, 1B was capable of causing the appearance of GCIs in the anterior commissure (AC) of wild-type mice[15], *i.e.*, in a major myelinated tract containing densely packed rows of interfascicular OLs. The dynamics and the prominence of the GCI pathology seeded in this tract supported the notion that like in MSA[32,33], the aSyn pathology seeded by 1B fibrils originated in neurons and was secondarily propagated to OLs[15].

After 24 months, a proper "invasion" of the posterior limb of the AC and of the bed nucleus of the *stria terminalis* (BNST) by GCIs could be observed (**Fig. 1a-e**), while Iba1-positive microglia did not particularly cluster around aSyn inclusion pathology (**Fig. 1c,d**). Confocal 3D volume reconstructions of affected OLs in the BNST showed the typical "flame-like" cytoplasmic distribution of phosphorylated aSyn (**Fig. 1e**). Global distribution of GCIs in full horizontal sections of mouse brain from animals sacrificed 1.5, 12, or 24 months after 1B fibril injection in their right caudate putamen (CP) showed generalized spread of GCIs (**Fig. 1f,** green markers). This was particularly prominent in the animal sacrificed at 24 months: in addition to the AC and to the BNST, GCIs were found bilaterally in deep cortical layers and the subcortical white matter, the CP, and unilaterally in the *globus pallidus* (GP) (injection side), the internal capsule (injection side), the entopeduncular nucleus (injection side), the *substantia nigra* (SN) *pars reticulata* (injection side), and the medullary reticular nucleus (contralateral side). A hovering section overview corresponding to **Fig. 1** can be found in the supplementary data.

At an earlier time point (17 months post-injection) and with 1B inoculation in the right SN, GCIs were seen particularly prominent in the *pars compacta* (SNpc), where a depletion of tyrosine hydroxylase signal was observed (**Extended Data Fig. 1a-f**). Numerous GCIs were found in the right SNpc (**Extended Data Fig. 1a, b, d, e**) but absent in the left SNpc (**Extended Data Fig. 1a, c, d, f**). Iba1-positive microglia were also found without obvious signs of clustering around aSyn inclusion pathology (**Extended Data Fig. 1d, e, f**). The anatomical spread of GCIs after intranigral injection of 1B remained lateralized in the forebrain and midbrain, where it mostly concerned the ipsilateral SN, internal capsule, entopeduncular nucleus, and GP, while it appeared bilateral in the brainstem (**Extended Data Fig. 1g**). It is worth noting that depending on the neuroanatomical structure and the time point under consideration, experimental GCIs coexisted with a variable load of surrounding neuronal aSyn inclusions (NCIs, NIIs or LNs), which represent the forefront of the aSyn pathology at earlier time points to progressively make way to a growing population of GCIs[15,23] (see also **Extended Data Fig. 1 h).**

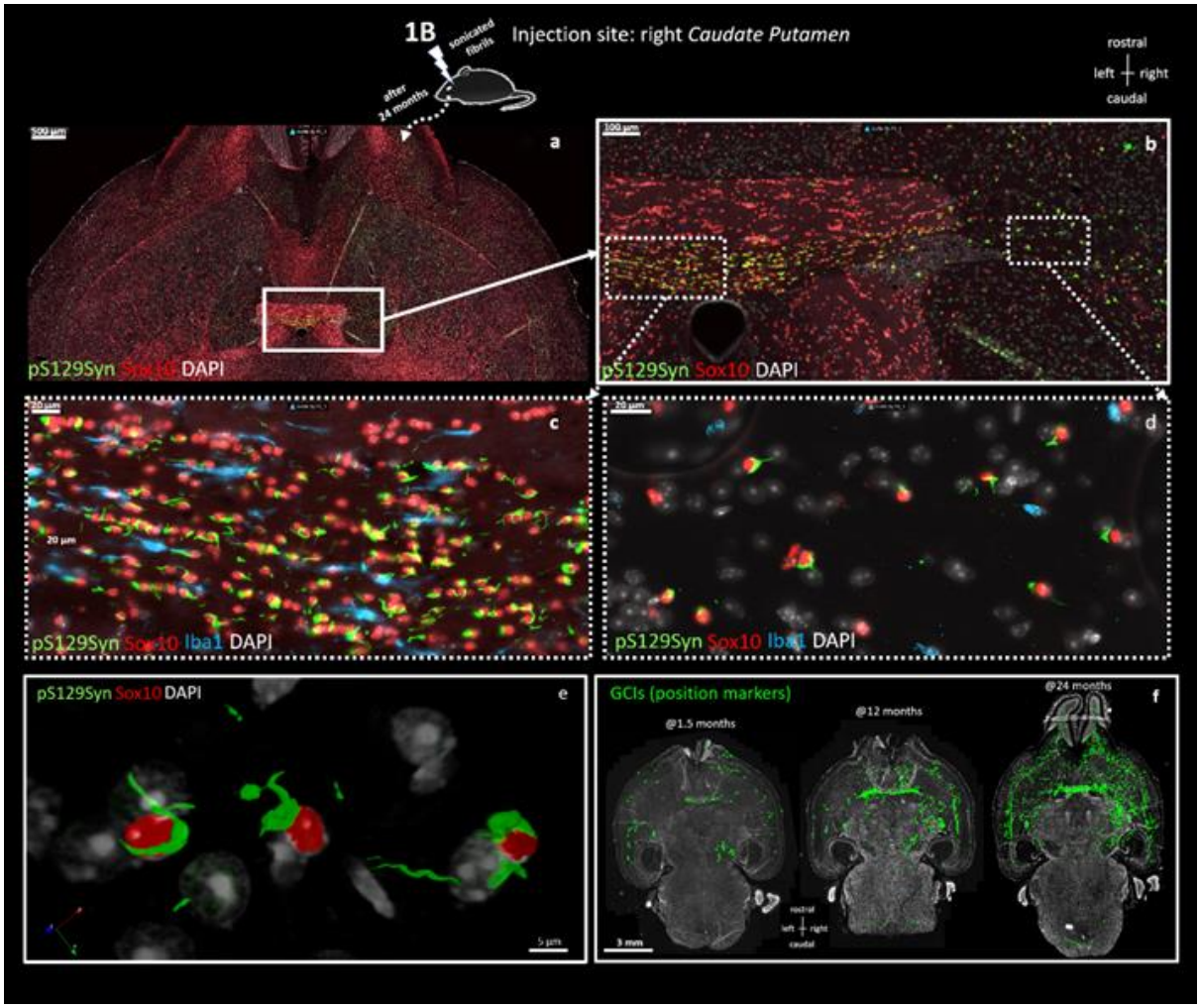

Fig. 1 | Seeding of GCIs in wild-type mice by alpha-synuclein fibrils from the 1B strain *(For red-green color-blind readers, see alternative color version in supp. data section).* ***a.*** *topographic immuno-fluorescence view of a horizontal brain section from a wild-type mouse injected 24 months earlier at the level of its right CP with 1B fibrils. aSyn inclusions are revealed using the anti-phospho aSyn antibody #64 (green), OLs by an antibody against the OL nuclear marker Sox10 (red), and nuclei using DAPI (white). The sectional plane intercepts horizontally the AC and the BNST (plain box)* ***b.*** *Higher magnification of the latter box evidencing the specific invasion by aSyn inclusions of the posterior limb of the AC (left dashed box), and of the BNST (right dashed box).* ***c.*** *Higher magnification of the left dashed box in (b): interfascicular OLs populating the posterior limb of the AC bear aSyn inclusions, i.e., GCIs, and sparse microglial cells are revealed using an antibody against Iba1 (blue).* ***d.*** *Higher magnification of the right dashed box in (b): satellite Sox10-positive OLs populating the BNST bear aSyn inclusions, i.e., GCIs, and sparse Iba1-positive microglial cells are detectable.* ***e.*** *Bird's eye view of a confocal 3D volume reconstruction centered on 3 OLs of the BNST bearing GCIs, from the section shown in (a). See also* ***Supplementary data movie 1****.* ***f.*** *Neuroanatomical distribution of GCIs in the brain of mice at 1.5, 12 and 24 months post-1B injection in their right CP. Full brain horizontal sections. The 24-month section is the n+1 section adjacent to the one shown in (a). Scale bars: in a = 500 µm; in b = 100 µm; in c, d = 20 µm; in e = 5 µm; in f = 3 mm.*

1B fibril structure determination and analysis

We previously observed a typical rod-like compact appearance for 1B fibrils with a fibril width compatible with the intertwining of two protofilaments using negative-stain transmission electron microscopy (TEM)[13]. In this study we additionally identified a characteristic left-handed helicoidal assembly using atomic force microscopy (**Extended Data Fig. 2a**).

We next analyzed the 1B fibrils with cryo-EM and determined the structure at a resolution of 1.94Å (**Fig. 2, Extended Data Fig. 2b-e**). We found that they corresponded to the characteristic twisting of two identical amyloid protofilaments with a pseudo-Greek-key motif consisting of 9 beta-sheets. These lack C2 symmetry but are related by an approximate 2_1 screw symmetry. The electron density map covers the sequence from G36 to K97, with an additional density attached alongside the starting sequence from G36 to V40 and reaching toward the inside of the protofilament interface. As that electron-density could not be unambiguously assigned to any sidechains, we did not build an amino acid sequence for this stretch. Both identically arranged protofilaments form their longest beta-sheet secondary structure from amino acids V52 to K58. Along this stretch is the main protofilament-protofilament interaction, where the fibrils are held together by electrostatic interactions with the opposite strand. The main electrostatic clusters are a positive group formed by K43, K45, and H50, and a negative group formed by E57 and T59, flanking the beta-sheet. Additionally, H50 appears to make an inter-rung connection within the same protofilament to the following subunit along the Z-direction to K45. The interaction between H50 and E57 causes the protofilaments to arrange in a half-step of the typical helical rise, by binding the next aSyn subunit of the opposite strand at the 2.36Å and a resulting twist of 179.52 degrees.

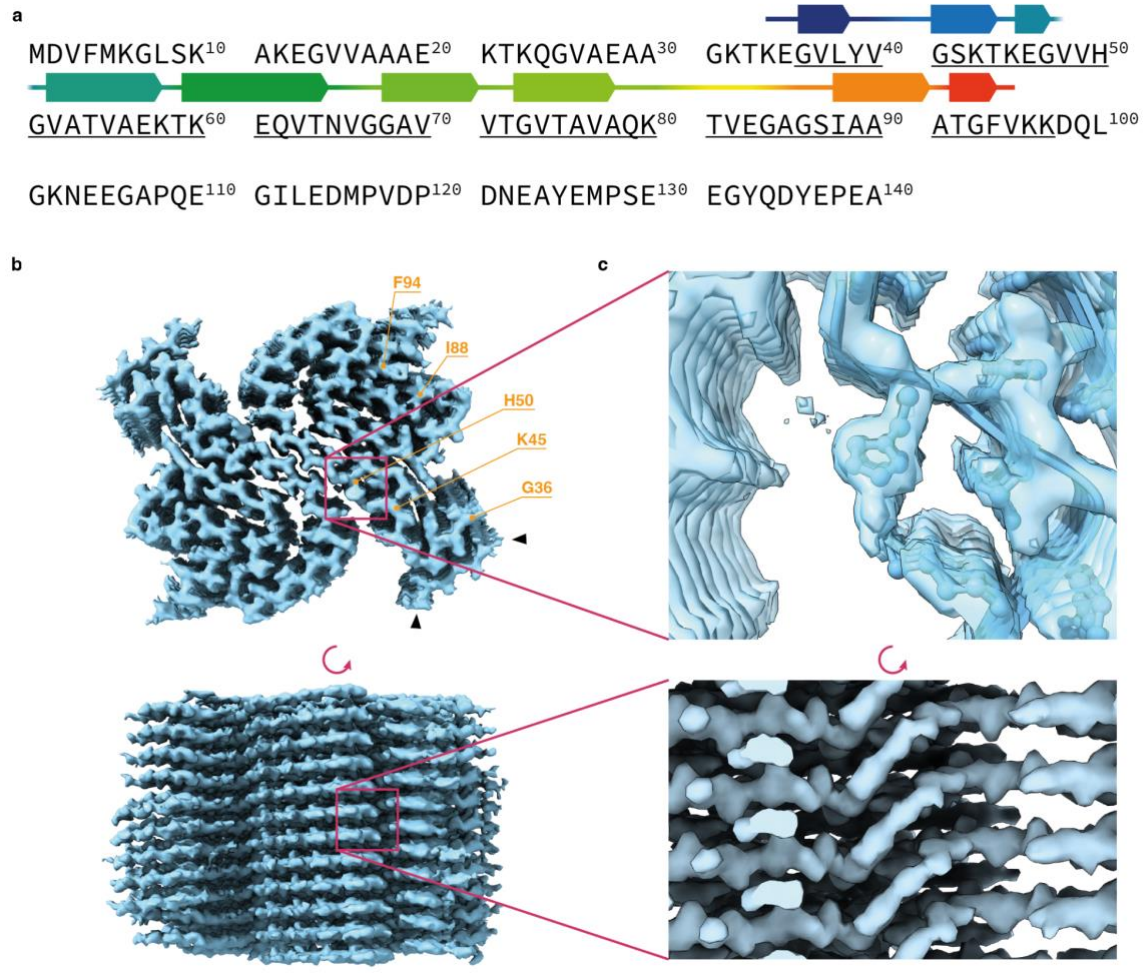

Fig. 2 | Structural organization of the 1B alpha-synuclein fibrils. a. *Amino acid sequence of wildtype aSyn indicating the resolved electron density map from K34 to V95. The different beta-sheets are indicated by the ribbon schematic above the single letter code.* ***b.*** *Top: Cross-sectional view of the electron density map of the 1.94Å resolution. Indicated are the starting position of G36, the K45 to H50 inter-rung connection, and the C-pocket relevant I88, and F94. The additional density along the starting stretch of G36 to V40 is indicated by the black arrowheads. Bottom: The side view of the structure.* ***c.*** *Zoom onto the H50 position, verifying the wild-type sequence (top) and visible inter-rung connection from the side view (bottom).*

The fundamental organization of a single protofilament shows distinct similarities to already published structures, mainly the patient-purified MSA fibrils[11] (PDB: 6XYQ), the corresponding amplification[12] (PDB: 7NCK), the H50Q variant[34] (PDB: 6PEO), and wt- and 1-121 aSyn variants[27,35] (PDB: 80QI and 6H6B) (**Fig. 3**). Observation of the Greek-key superimposition of the similar models indicates the identical arrangement of I88 and F94, previously reported as the C-pocket and binding site for ThT[16], in only a subset of structures and particularly in MSA fibrils (PDB: 6XYQ and PDB: 7NCK) and the H50Q variant (PDB: 6PEO). This is notable because like the 1B fibrils, H50Q fibrils (PDB: 6PEO) are ThT negative[34]. Consequently, the inaccessibility of the I88 pocket seems important to account for the ThT-negativity of 1B fibrils (**Fig. 3b**).

In addition, the other ThT binding pocket located at the N-terminus (N-pocket)[16] of the fibrils also shows a modification compared to ThT-positive fibrils, by having a shift of Y39 so that it faces T44 and E46 and is no longer available for interaction with ThT within the N-pocket[16]. Note that a similar conformation of the N-pocket with "shifted" Y39 presumably preventing ThT binding is also observed in the amplified MSA fibrils (PDB: 7NCK)[12] and the H50Q mutation (PDB: 6PEO), again in line with the parallel observation that seed amplification products templated on MSA brain extracts or on MSA cerebrospinal fluid are ThT-negative[26].

Collectively, these data support the hypothesis that closure and distortions of the ThT-binding pockets at the surface of the fibrils can explain the phenomenon of "ThT invisibility" and at the same time establish important structural determinants of the pathophysiological specificity of both 1B and MSA fibrils.

Besides regions involved in ThT binding, comparison with the other aSyn fibril folds also indicates the near identical arrangement of the H50Q variant to the 1B structure, with the exception of the H50 inter-rung side-chain orientation due to the point mutation. Whether this orientation is important and confers specific "MSA-like" properties to 1B is unknown, especially since the >3Å resolutions of PDB: 6XYQ and PDB: 7NCK do not allow conclusions on its existence in the MSA fibrils.

The 1B fibril structure also shows an outer, non-identified density stretch interacting with G36 to V40 (**Fig. 2b**), a feature which is also present in fibrils amplified from MSA (PDB: 7NCK) and in H50Q fibrils (PDB:6PEO). This is remarkable, because this outer stretch blocks access of the disaggregase complex effector-component HSC70 to its binding site at the N-terminus of the fibrils, thus most probably preventing their disassembly and clearance[36]. This structural feature might thus represent a reason for the acute *in vivo* seeding capability of 1B[14].

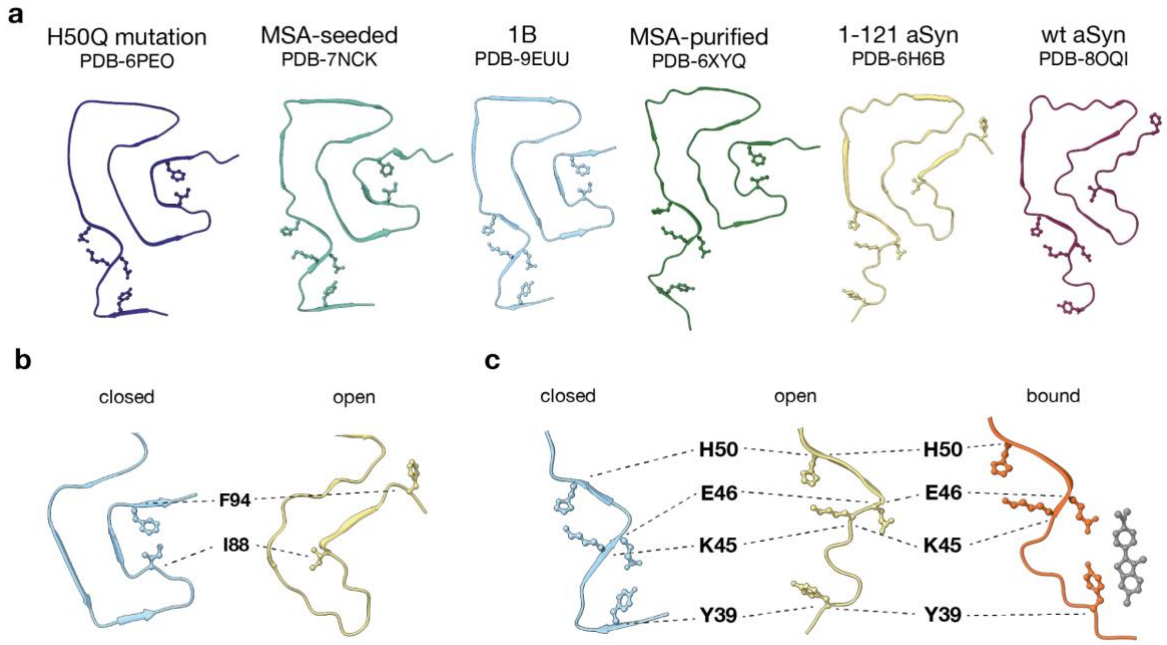

Fig. 3 | Structural diversity of aSyn fibrils. a. *Comparison of similar aSyn fibril structures. Indicated are Y39, K45, E46, H50, I88, and F94 along the sequence stretch, which define the open or closed state of either the C- or N-pocket.* ***b.*** *Zoomed view of the arrangement of the C-pocket on the example of 1B (left, PDB 9EUU) and 1-121 aSyn (right, PDB 6H6B).* ***c.*** *Zoomed view of the arrangement of the N-pocket on the example of 1B (left, PDB 9EUU), 1-121 aSyn (center, PDB 6H6B), and ThT-bound (grey) aSyn (right, PDB 7YNM).*

Tissue ultrastructure of 1B-induced neuropathology

We analyzed the cellular inclusions in affected mouse brains, using CLEM with an adaptation of our previously described protocol[37]. Consecutive mouse brain tissue slices were imaged by fluorescence microscopy to identify the slices with aSyn inclusions. These sections were then resin-embedded and heavy-metal stained in preparation for EM imaging. From the embedded sections, serial ultrathin sections were collected consecutively on glass slides and on EM grids, with the glass slides being used for immunohistochemistry to re-localize the aSyn positive cells and toluidine blue staining for optimal contrast of the sample. The resulting immunohistochemistry and toluidine blue images were then successfully correlated to EM images taken on the consecutive grids. We used an animal of the 1B-injected series corresponding to **Extended Data Fig. 1a-f**. We imaged 30 aSyn positive inclusions in a region straddling the right GP and CP and followed them throughout the brain tissue by serial sectioning. We could identify fibrillar material and membranous cytoplasmic sub-compartments in the aSyn-positive areas. For verification of the fibrillar morphology, we conducted room-temperature electron tomography on various positions within the IHC-positive regions of interest. Tomography data underscored the presence of fibrillar morphology in a dispersed, bundled, and clustered arrangement (**Fig. 4, Extended Data Fig. 4**). We additionally verified that the fibrillar material in the aSyn-positive IHC regions was aSyn protein, using immunogold labelling (**Extended Data Fig 3**).

The dispersed fibrillar material correlated with the aSyn-positive signal in the IHC image and could be found throughout all observed inclusions in the tissue. We measured the size of the nuclei of the pathological cells to be able to distinguish between NCIs and GCIs. Six pathological cells with nuclei of more than 8.5 µm diameter were assumed to be neurons with NCIs, and sixteen pathological cells with a nucleus size below 8.5 µm were assumed to be GCIs in OLs. In many cases, the correlated area consisted of dispersed fibrillar material within a membranous local environment with various vesicular compartments. Fibril bundles could not be observed in all inclusions. If they were present, they varied strongly in length, thickness, curvature, and localization within the cell. Measurement of the fibril

bundles in 23 inclusions throughout 5 brain slices showed an averaged fibril bundle length of 0.81 ± 0.41 µm. In most cases, the bundle length was of similar size of around 0.62 ± 0.07 µm. In a few exceptional cases, we measured bundles with individual lengths of 1.08 µm up to 3.64 µm (**Fig. 4a**). Fibrils in bigger clusters irregular arrangements, in a chaotic overall fashion with individual radiating fibrils on the outside (**Fig. 4b**).

In addition, we could observe the regular proximity or direct contact of different and morphologically distinct cells to pathological ones (**Extended Data Fig. 5**). The morphology of these cells is reminiscent of cells described as "dark microglia" in mouse models for Alzheimer's disease[38,39], as well as of cells recently described in human post-mortem MSA brain[40].

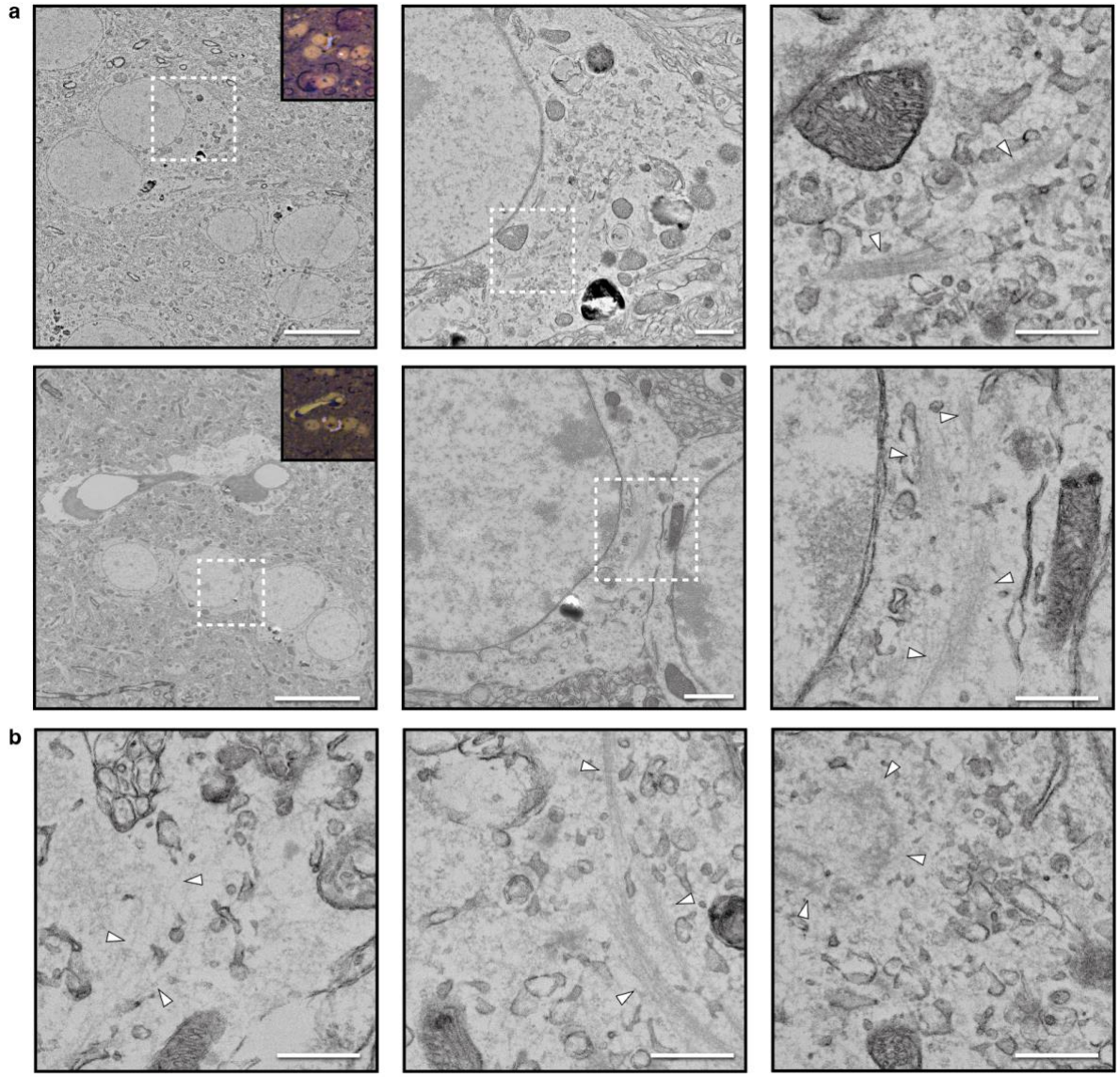

Fig. 4 | Tissue ultrastructure of 1B-seeded mouse brain. a. *Correlative light and electron microscopy analysis of aSyn positive regions. From left to right: overview EM image (scale bars = 10 µm); closer view at the pathological region at the indicated area (scale bars = 1 µm); and high magnification at settings taken for tomography to verify fibrillar material (scale bars = 500 nm). Fibril pathologies are indicated by arrowheads. Insets in the left panels show the same locations as IHC and toluidine blue light microscopy image with the pathology in inverted color as a bright blue feature.* ***b.*** *High magnification EM images of different types of fibril arrangements, indicated by arrowheads. From left to right: "dispersed", "bundled", and "clustered" (scale bars = 500 nm).*

Seeding compliance of aSyn variants towards 1B

The *in vivo* formation of fibrillar GCIs seeded in non-transgenic mice by human 1B fibrils requires templating and fibril replication, during which endogenous mouse aSyn monomers are recruited to the elongating assemblies. Templating appears here to accommodate the threonine at position 53 in mouse aSyn, even though the 1B seed is formed by human aSyn that has an alanine in that position 53. This is remarkable, since a faithful replication of the double protofilament structure of 1B is difficult to conceive in light of the steric clash of T53 with the structure. The protofilament interface of 1B at the position of A53 does not provide enough space for the side chain of a threonine to fit[41]. It therefore seems likely that during the formation of GCIs in mice, the interface of the neo-fibrils seeded by 1B either may be absent, like in the synthetic H50Q narrow fibrils[34], or that an alternative protofilament interface is established, like in the synthetic A53T fibrils[42].

Given this observation, we asked whether other pathological aSyn mutations affecting residues involved in the establishment of the protofilament interface of 1B could as a general rule prove neutral to the process of inclusion seeding by 1B fibrils. To investigate this, using AAV vectors, we expressed wild-type human aSyn or aSyn variants carrying the mutations A53T, H50Q, G51D, or A53E, in 96-well primary cultures of cortical neurons[13,14] from aSyn KO mice. Additionally, we exposed these infected neurons to 1B fibrils to template the aggregation of the different aSyn variants. For comparison, we also expressed aSyn with the E46K mutation, which does not localize to the protofilament interface but should be incompatible with the replication of the pseudo-Greek-key motif of 1B, and aSyn with the A30P mutation, which is neither relevant to the interface nor to the pseudo-Greek-key motif.

Confirming our previous considerations about T53, quantification of aggregation 23 days after seeding indicated that none of the "interface mutations", nor the A30P mutation reduced the aggregation process triggered by 1B. Only the E46K mutation, which prevents the formation of the E46-K80 salt bridge that stabilizes the pseudo-Greek-key fold of 1B, almost completely abrogated seeded aggregation (**Fig. 5a,b**).

This supports the idea that replication of the protofilament interface is generally dispensable for 1B to seed GCIs in mice.

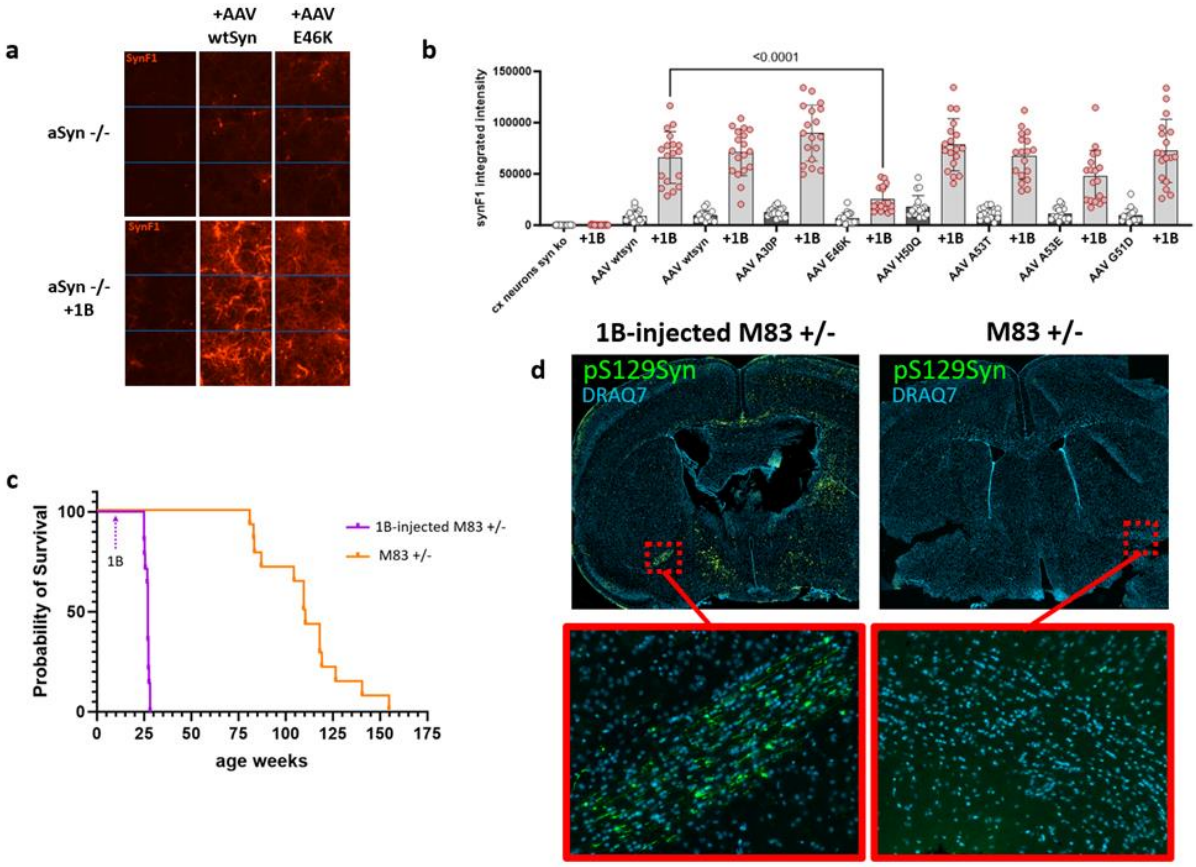

Fig. 5 | Inclusion seeding by "1B" fibrils is inhibited by E46K, but not by aSyn mutations affecting the protofilament interface and is rapidly lethal in hemizygous transgenic mice expressing human A53T aSyn. ***a.*** *96-well pooled primary cultures of cortical neurons from 8 aSyn-KO mouse embryos were challenged or not at day-in-vitro 7 (DIV7) with 10 nM 1B fibrils (equivalent aSyn monomer concentration), and infected or not with AAV-aSyn or AAV-E46K aSyn at DIV11. The neurons were fixed at DIV30 and the aSyn inclusions revealed using the conformation-dependent antibody SynF1 (red); three immunofluorescence fields of views (FOVs) imaged in a test well for each condition, illustrate: (i) the absence of SynF1 signal at DIV30 in the absence of endogenous aSyn, (ii) aSyn inclusion seeding by 1B in conditions of aSyn expression, and (ii) a minor inclusion seeding when E46K aSyn is expressed instead of wild-type aSyn.* ***b.*** *High Content Analysis of the experiment shown in (a) and extended to a series of aSyn mutants based on 18 FOVs from 6 wells for each condition. The AAV-aSyn condition was doubled to document robustness. One-by-one comparisons to wild-type aSyn reveals that E46K aSyn is the only mutation reducing the compliance to inclusion seeding by 1B (mean value comparison, Student's t-test, $p<0.0001$).* ***c.*** *Kaplan-Meier survival curves of 28 hemizygous transgenic mice expressing human A53T aSyn (M83 +/-) without (14 mice, orange curve) of after (14 mice, purple curve) a unilateral injection (right CP) of 1B fibrils (time of injection: arrow).* ***d.*** *Illustrative concatenated immunofluorescence views of coronal brain sections of a 1B-injected M83 +/- mouse at the time of death (left), and of a M83 +/- mouse of similar age (right). Red boxes: zoomed views centred on the posterior limbs of the AC. aSyn inclusions are revealed using the anti-phospho aSyn antibody EP1536Y (green), nuclei are revealed with DRAQ7 (blue).*

To further challenge this assumption using an *in vivo* model, we inoculated our 1B fibrils into hemizygous transgenic M83 mice expressing human A53T aSyn. These hemizygous mice have a normal lifespan, despite the presence of one copy of the human aSyn A53T transgene[9,10]. These mice showed to be replication-compliant for MSA prions that were isolated from human patients, and these prions induced death in the mice in only a few weeks after intracerebral injection[9,10]. Thus, if our conclusions were correct regarding (i) the non-mandatory establishment of an inter-protofilament interface for GCI seeding by 1B, and (ii) the analogy of the structure of 1B with the natural MSA prions, then we should expect to observe an impact of intracerebral injection of 1B on the longevity of these M83 hemizygous mice "in spite" of the presence of the A53T mutant aSyn.

We found that the intracerebral injection of 1B fibrils in the M83 hemizygous mice caused their death in a strikingly synchronized fashion after only 16 weeks (**Fig. 5c**). This was associated with the appearance of numerous intracerebral aSyn inclusions, in particular in the posterior limb of the AC, in which the presence of Lewy neurite bundles and GCIs could be observed (**Fig. 5d**). Non-seeded control M83 mice of similar age were healthy and showed no intracerebral aSyn inclusions (**Fig. 5d**). This experiment indicates that like MSA prions isolated from patients, 1B fibrils cause the premature and synchronous death of hemizygous M83 mice expressing human A53T aSyn, irrespective of the negative impact of the mutation on the templated replication of the protofilament interface[42].

It is important to highlight here that while GCIs do constitute a hallmark of MSA compared to other sporadic alpha-synucleinopathies, this no longer holds true when considering inherited Parkinson's disease (PD). Indeed, at variance from the sporadic cases of PD in which GCIs are rarely observed[3], the patients bearing the germline aSyn mutations A30P [43], A53T [44], A53E [45] or G51D [46] all present GCIs. These three latter mutations interfere directly with the formation of a protofilament interface similar to the one seen in 1B[42,47,48]. It is thus tempting to speculate that the loss of the interface in the neo-fibrils seeded *in vivo* by 1B, far from impeding their spread, might on the contrary be an important component of their capability to seed the formation of GCIs.

The likely loss of protofibril interface during the templating of 1B *in situ* in the wild-type and M83 transgenic mice could be used to argue that other structural features of the input fibrils might be lost as well. Two observations tend to contradict this assumption: first, it has been shown that the *in vitro* replication of MSA fibril "case 5" proceeds with a complete loss of protofilament interface and still yields a single protofilament product that is a faithful copy of the one contained in the original MSA assembly[12], and which is similar to those found in 1B fibrils. Second, we observed that the E46K aSyn mutation was capable of preventing 1B replication in neurons, while other familial PD aSyn mutations were not: this indicates that for the replication of 1B to take place, correct templating of the pseudo-Greek-key fold is not facultative and cannot be "bypassed". This parallels the observation that the *in vivo* replication of MSA prions extracted from diseased brains is not affected by A53T and A30P mutations, while it is inhibited by E46K[49,50]. Thus, the *in vivo* replication of MSA prions and that of 1B fibrils are both insensitive to aSyn mutations affecting the templating of the protofilament interface and are both sensitive to the E46K mutation. This completes the picture of the structural similitude of the aSyn fibrils present in MSA with our synthetic strain 1B by also highlighting the analogy of the templating compliance of distinct aSyn variants towards 1B and MSA prions[49,50].

1B as a synthetic MSA prion

To challenge the concept that 1B can indeed be considered a synthetic MSA prion, we studied its capacity to be passaged *in vivo* in M83+/- mice, and to subsequently maintain its seeding activity in wild-type mice (**Fig. 6**). To check this possibility, the brains of diseased M83+/- mice due to a prior inoculation with 1B fibrils were simply homogenized, diluted, and re-inoculated without further processing to wild-type mice. The same experiment was performed in parallel with the brains of diseased M83+/- mice that underwent a prior inoculation with either a human MSA brain homogenate[51] or with a brain homogenate from spontaneously diseased M83+/+ mice[51]. The results indicate that (i) only the MSA brain homogenates and the 1B fibrils present a seeding activity in wild-type mice after passage in M83+/- mice (**Fig. 6 and Extended Data Fig. 6**), and that (ii) the intracerebral aSyn pathology spread patterns of passaged MSA and 1B look strikingly similar (**Fig. 6**), with the formation of prototypic aSyn inclusions (**Extended Data Fig. 6** and corresponding 3D reconstructions in supplementary data section). This identifies 1B with a synthetic MSA prion capable of animal-to-animal transmission without extraction and/or concentration procedures. This goes one step beyond the passage properties originally described by Prusiner and his group for natural MSA prions[9,10,49] and was never reported before for any alpha-synucleinopathy - human or experimental - using crude brain homogenates as a vector of transmission to non-transgenic animals.

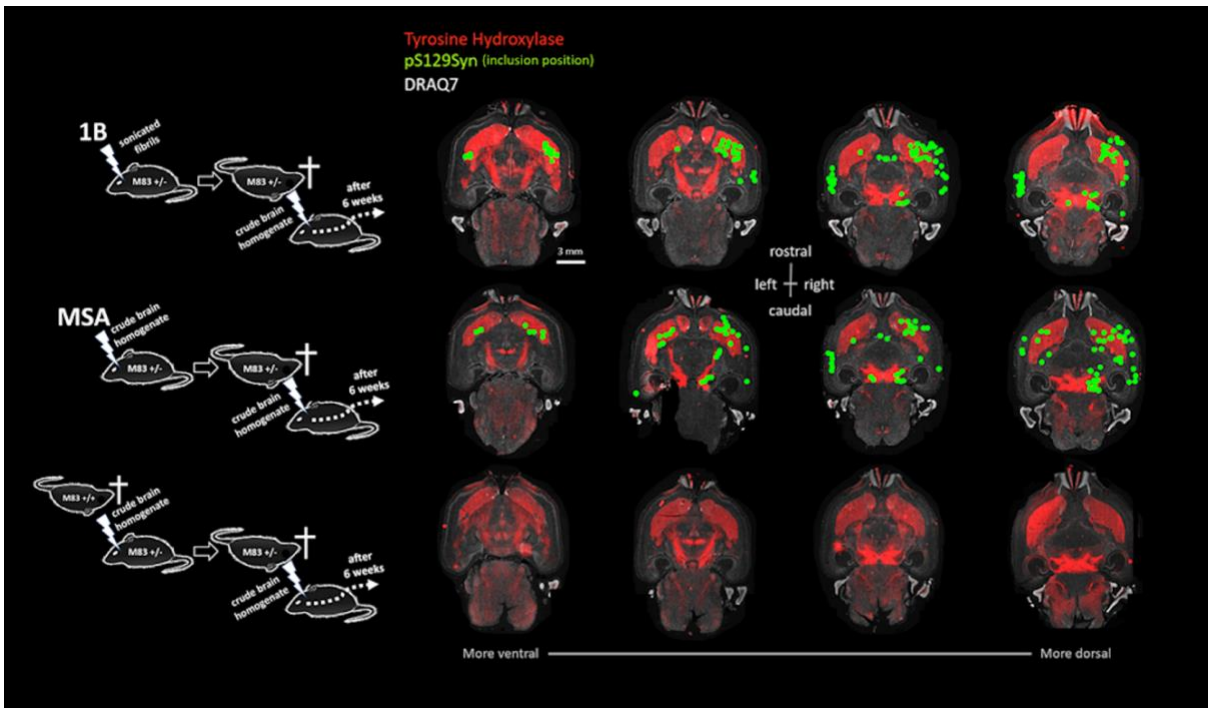

Fig. 6 | Animal-to-animal transmission of 1B and MSA aSyn pathology by crude brain homogenates *(For red-green color-blind readers, see alternative color version in supp. data section). Diluted crude brain homogenates were prepared from prematurely dying M83+/- mice that had been previously injected either with human 1B fibrils (upper row), or with a brain homogenate from a deceased MSA patient[51] (middle row), or with a brain homogenate from a spontaneously dying homozygous M83+/+ transgenic mouse (bottom row). The corresponding brain homogenates were injected in the right CP of 6 wild-type mice (2 per group). After 6 weeks, wild-type mice were sacrificed, and their brains were processed for horizontal sectioning and immunofluorescence neuropathology. aSyn inclusions were revealed using an anti-phospho aSyn antibody (EP1536Y, green), the nigrostriatal tract was evidenced using an anti-Tyrosine Hydroxylase antibody (TH, red) and the nuclei were revealed with DRAQ7 (white). 3 animals are displayed with 4 sections for each, sampling the nigrostriatal tract along its dorso-ventral axis. Green dots materialize the position of the aSyn inclusions in the sections (Lewy neurites, NCIs, NIIs, GCIs and GNIs). Note the strikingly analogous anatomical spread patterns in the 1B and MSA conditions and the absence of pathology in the « M83-only » condition. Scale bar = 3 mm.*

Discussion

We presented here the high-resolution structure of aSyn fibrils 1B and report their capability to induce prion-propagated MSA pathology through seeding in mice. These fibrils were discovered by serendipity as "ThT-negative" fibrils, endowed with the capability to induce aSyn inclusion pathology both *in vivo* and *in vitro.* As previously shown, seeding with 1B causes the formation of Lewy neurites, NCIs, NIIs and GCIs. Here, we present the fibrillar ultrastructure of NCIs and GCIs seeded *in vivo*, 17 months after an intracerebral injection of 1B. Besides seeding with 1B fibrils, the capability of inducing the formation of GCIs with synthetic material was previously only reported twice, and interestingly, in both cases using ThT-negative fibrils as well. This lets us hypothesize that accessibility of a specific ThT-binding site along I88 is incompatible with a disease-relevant MSA fibril strain. The specific binding site around the C-pocket of I88 is closed by forming a "lever" with F94. This is mainly due to the outward orientation of I88 in comparison to other, similar, structures. The inner "hook" of the pseudo-Greek-key motif along the stretches of V74 to F94 is shifted by one amino acid position starting at A85. As a result, A85 points outwards at the most prominent position of the inner hook, which causes a consequential inversion of sidechain positioning for the remaining sequence. This causes S87, a known modification site for fibril inhibition by O-Glc-N acylation[52] or by phosphorylation[53] to be inaccessible, and I88 to be positioned outwards, undergoing a connection with F94 and therefore closing the C-pocket for ThT-binding. Strikingly, this feature of a closed C-pocket is also found in human aSyn fibrils directly purified from human MSA patients[11], mirroring the observation that seed amplification assays performed on MSA samples yielded ThT-negative fibrils[26] as well. It is interesting to note that ThT-negativity is also associated with C-pocket closure in the H50Q variant characterized by Boyer et al.[34] and importantly, that we can allocate the ThT-negativity of the 1B fibrils to the homogeneity of our sample, as indicated by the 3D classification averages during processing of cryo-EM images (**Extended Data Fig. 2b**). We argue that the structural homogeneity of the fibrils, which implies an absence of fibril polymorphism, is a necessary condition to rule on ThT-negativity. This, combined with the *in vivo* GCI seeding capability of 1B fibrils, suggests a potential biological and pathophysiological importance of the closed C-pocket with direct relevance to MSA. This suggests that interfering with this site could represent a valid therapeutic strategy in which altering the state of C-pocket accessibility would modulate 1B fibril templating and replication *in vivo*.

An unanswered structural question is the identity of the additional density in the fibrils found adjacent to the aSyn sequence G36 to V40. As this density is likely hindering the binding of HSC70 to the N-terminal region of the fibril[36], the resulting inhibition of fibril disassembly and clearance by the disaggregase complex might significantly contribute to the toxicity and templating effect of this aSyn strain. We hypothesize that this, together with the C-pocket closure, underlies the prion-like behavior of the 1B fibrils.

The inter-rung connection established between H50 and K45 is a remarkable feature of the 1B fibril polymorph. It may contribute to its stability and foster fibril templating and toxicity. Additionally, the overall protofibril interface is distinct in comparison to already published structures. It is formed along V52 to K58 and held together by the interaction of the flanking electro-positive and -negative clusters with the opposite strand.

The presence of seeded fibrils in the GP and CP in the fixed mouse brain tissue indicates that the 1B fibrils replicate according to a prion-like mechanism. The location of fibrillar structures seen by EM correlated with positive phosphorylated aSyn immunostaining, allowing their unambiguous identification. As we find the fibrillar material in a dispersed, bundled, or clustered morphology, we suspect that besides seeding, continuous processing of fibril material both in neurons and OLs participates in the maturation of NCIs and GCIs. The regular presence of morphologically distinct cells close to the pathology is reminiscent of previously reported microglial recruitment around amyloid plaques in AD mouse models[38,39]. This is intriguing, because we did not find a correlation of the spatial distribution of Iba1-positive cells with that of cells bearing aSyn inclusions in our immunofluorescence observations (**Fig. 1**). However, Iba1-negative microglia do exist[38] and could thus correspond to the cells lining the neurons and oligodendrocytes bearing NCI and GCIs in our experiments. Nevertheless,

more insight into the presence of these "lining" cells is needed and should be investigated in future work.

Finally, it is striking that beyond the structural similarities of 1B and MSA fibrils, the compliance of aSyn mutations towards the seeding of aSyn inclusions by 1B fibrils is also similar to those described for "MSA prions" by the group of Prusiner [9,10,49]. Of note, the latter claim of analogy with prions is further substantiated for both 1B and MSA fibrils, by our observations of effective animal-to-animal pathology transmission and using unprocessed brain homogenates as vectors. It is therefore important that in the absence of prior knowledge of the synthetic aSyn or patient-derived fibril polymorph, this type of material should be handled with strict precautions and effective personal protection measures.

Altogether, we present the high-resolution fibril structure of the "1B" fibril strain capable of seeding GCIs and NCIs in the mouse brain according to a prion-like mechanism. Additionally, we present the ultrastructure of these seeded inclusions using RT-CLEM and show that they are populated by dispersed, bundled, and clustered aSyn fibrils. Together, the high resolution achieved and the ultrastructural insights in mouse brain, highlight the similarity of 1B and MSA fibrils, and postulate a link between fibrillar structure, assembly, resistance to clearance, mechanism of prion-like seeding and spreading, and animal-to-animal transmission.

Online methods

α-Syn expression

Escherichia coli strain BL21(DE3) was transformed with pT7-7 aSyn wt vector[54] from Addgene, deposited by Hilal Lashuel (Addgene plasmid #36046; http://n2t.net/addgene:36046; RRID: Addgene_36046) and plated onto a Luria broth (LB) agar plate containing ampicillin (100 µg/mL) and 1 g/L glucose. A preculture in 5 mL of LB medium was inoculated with one clone and incubated at 37°C under 200 rpm shaking for 4 h. Cells from the LB preculture were recovered by centrifugation (1000× g, 10 min) and used for inoculating 200 mL of LB medium. Cells were grown overnight at 37°C under 200 rpm shaking and then diluted in 2 L of culture. Protein expression was induced by adding 0.5 mM isopropyl-β-d-thiogalactopyranoside during the exponential phase, evaluated at an optical density at 600 nm reaching 0.6. Cells were harvested after 5 h of culture at 30°C by a 7000× g centrifugation at 4°C, 20 minutes (JLA 8.1000, Beckman Coulter, Villepinte, France), and pellet was kept at −20 °C until purification.

α-Syn purification

The pellets were resuspended in lysis buffer (10 mM Tris and 1 mM EDTA (pH 7.2) with protease inhibitor tablets (cOmplete, EDTA-free protease inhibitor cocktail, Roche, Basel, Switzerland) and sonicated at 50% max energy, 30 s on and 30 s off for three rounds with a probe sonicator (Q-Sonica, Newtown, CT, USA). The sonicated pellets were centrifuged at 20,000× g for 30 min, and the supernatant was saved. The pH of the supernatant was then reduced to pH 3.5 using HCl, and the mixture stirred at room temperature (RT) for 20 min and then centrifuged at 60,000× g for 30 min. The pellets were discarded. The pH of the supernatant was then increased to pH 7.4 with NaOH and then dialyzed against 20 mM tris-HCl (pH 7.4) and 100 mM NaCl buffer before loading onto a 75 pg HiLoad 26/600 Superdex column equilibrated with the same buffer with ÄKTA pure system. Monomeric fractions were collected and concentrated if needed by using Vivaspin 15R 2 kDa cutoff concentrator (Sartorius Stedim, Göttingen, Germany). Purification fractions were analyzed by polyacrylamide gel electrophoresis (PAGE) tris-tricine 13% dying with ProBlue Safe Stain. Protein concentration was evaluated spectrophotometrically by using absorbance at 280 nm and an extinction coefficient of 5960 M^{-1} cm^{-1}. Quantification of the preparations with a Pierce chromogenic LAL kit indicated a low endotoxin [lipopolysaccharide (LPS)] residual value of 0.03 to 0.06 EU per µg of recombinant protein.

α-Syn fibrillization

Solutions of monomeric α-Syn at 4 to 5 mg/mL in saline (H2O, 100 mM NaCl, and 20 mM tris-HCl pH 7.40) were sterilized by filtration through 0.22 µm Millipore single-use filters and stored in sterile 15 mL conical falcon tubes at 4°C. Sterilized stock was then distributed into safe-lock Biopur individually sterile-packaged 1.5 mL Eppendorf tubes as 500 µL aliquots and were seeded with 1% of 1B strain fibrils[13–15]. The tubes were cap-locked and additionally sealed with parafilm. All previous steps were performed aseptically in a particle-free environment under a microbiological safety laminar flow hood. The samples were loaded in a ThermoMixer (Eppendorf, Hamburg, Germany) in a 24-position 1.5 mL Eppendorf tube holder equipped with a heating lid. Temperature was set to 37 °C, and continuous shaking at 2000 rpm proceeded for 4 days. 1B templating of the fibrillization products was quality-checked using the fibrilloscope[13–15].

Sonication

Prior to intracerebral injections, 1B aSyn fibril stocks (4 mg/mL) were distributed in cap-locked, sterile 0.5 mL polymerase chain reaction (PCR) tubes (Thermo Fisher Scientific, Bordeaux, France). Sonication was performed at 25 °C in a Bioruptor Plus water bath sonicator (Diagenode, Liège, Belgium) equipped with thermostatic control and automated tube carousel rotator. The sonication power was set to “high”, and 10 cycles of 30 s on followed by 10 s off were applied.

In vivo α-Syn pathology

Adult 129SV (intrastriatal injections), C57BL/6 (nigral injections), and transgenic M83 (hemizygous, intrastriatal injections) were housed in a temperature-controlled (22 °C) and light-controlled environment on a 12 h light/12 h dark cycle with access to food and water ad libitum. The study design was approved by the French Ministry of Research and all experimental procedures were conducted in accordance with the European Communities Council Directive (2010/63/EU) for care of laboratory animals. The mice (6–8 weeks old) unilaterally received 2 µL of sonicated α-Syn fibrils 1B (4 mg/mL) by stereotactic delivery at a flow rate of 0.4 µL/min, and the pipette was left in place for 5 min after injection to avoid leakage. Delivery was performed within the right striatum (coordinates from bregma: AP, −0.1; L, +2.5; DV, +3.8), or above the right substantia nigra (coordinates from bregma: AP, −2.9; L, −1.3; DV, −4.5). Wild-type mice (n=20) and transgenic M83 hemizygous mice (n = 28) injected with either PBS, 1B fibrils, or brain homogenates were euthanized after 6 weeks, 17 months, 24 months, or when reaching the humane endpoints defined as death regarding the transgenic M83 mice, and were transcardially perfused with either tris-buffered saline (pH = 7.4) followed by 4% paraformaldehyde in PBS pH = 7.4 at 4 °C, or with cacodylate buffer 0.1 M with 1 mM $CaCl_2$ (pH = 7.4) followed by 4% paraformaldehyde plus 0.1% glutaraldehyde in 0.1 M cacodylate buffer (pH = 7.4). Brains were subsequently postfixed in the same fixative. For standard neuropathology, the brains were paraffin embedded, and 10 µm sections were cut with a rotative microtome (Leica, Milan, Italy). The sections of interest were deparaffinized and processed for epitope retrieval: the slides were immersed in citrate buffer pH 6 (Dako Agilent Technologies, Les Ulis, France) and placed in a pressure cooker (Bio SB, Santa Barbara, CA, USA) at 120 °C for 10 min. After a cooling period of 20 min, the slides were washed twice for 5 min in PBS at room temperature. They were then processed for simple or double immunofluorescence using the following primary antibodies diluted at 1/500, or their combinations: EP1536Y (Abcam) or pSyn#64 (Wako) for detecting phospho-S129–positive aSyn inclusions; anti-Sox10 (Abcam, rabbit monoclonal) for detecting OL nuclei; EP1532Y and anti-TH raised in chicken (anti-Tyrosine Hydroxylase, Abcam) for detecting the nigrostriatal tract; and anti-Iba1 (Abcam) for detecting microglia. DRAQ7 or DAPI were used to image the nuclei. The AlexaFluor-coupled secondary antibodies were from Thermo Fisher (Alexa 488, 568, and 674). The sections were acquired using a Pannoramic slide scanner (3D HISTECH, MM France) in epifluorescence mode, and multichannel fluorescence optical sections of the samples were performed (thickness < 0.8 µm) using either a Zeiss CD7 platform of a Leica SP5 Laser Scanning Confocal Microscope equipped with a spectral detector, 488, 561, and 633 nm laser lines, a motorized X-Y stage, and a mixed stepping motor/piezo Z controller. The objective was 40×, and Z step size was set to 0.5 µm to produce stacks of 15 to 20 Z planes. Pinhole was set to 1 airy unit. For 3D reconstructions and volume rendering/animations (corresponding to 360° tilt series of composite max pixel projections images), raw 3-channel Z-stack images were processed offline using Icy[55].

High content analysis (HCA) of 1B-seeded aSyn inclusions in primary neuronal cultures expressing human aSyn and its variants

Timed inbred-pregnant C57BL/6JOlaHsd (aSyn KO) female mice were received from Envigo (Puteaux, France) 2 days before initiation of the primary culture. The pregnant mouse was euthanized by cervical dislocation, and the aSyn KO embryos (embryonic day 18) were surgically extracted and cold-euthanized. Cortices were harvested from 8 of them, pooled, and dissociated enzymatically and mechanically (using a neural tissue dissociation kit, C Tubes, and an Octo Dissociator with heaters; Miltenyi Biotech, Germany) to yield a homogenous cell suspension pool of 8 individuals. The cells were then plated at 20,000 per well in 96-well plates (Corning, BioCoat poly-d-lysine imaging plates) in neuronal medium (MACS Neuro Medium, Miltenyi Biotech, Germany) containing 0.5% penicillin-streptomycin, 0.5 mM alanyl-glutamine, and 2% NeuroBrew supplement (Miltenyi Biotech, Germany). The cultures were maintained with 5% CO2 at 37°C in a humidified atmosphere. The medium was changed by one-third every 3 days, until 30 DIV (days in vitro). In such cultures, and under control conditions, neurons represented approximately 85 to 95% of the cell population; thus, for simplicity, they are here referred to as “neurons.” After 7 DIV, vehicle and sonicated 1B aSyn fibrils were added at a final concentration of 10 nM equivalent monomeric concentration. When relevant, neurons were infected at DIV 10 with AAV (adeno-associated virus) particles (multiplicity of infection, 1000)

carrying the cDNA of aSyn and its variants under the control of the human synapsin promoter, as previously described[14]. High Content Analysis was performed after fixation and immunofluorescence staining as previously described on images acquired at 20× using the generic analysis module of an Incucyte S3 (Sartorius, USA) with Top-Hat segmentation based on the synF1 signal. For quantifications the signal integral of the segmented areas in each field of view was recorded.

Correlative light and electron microscopy

The CLEM protocol was performed as previously described[37]. In short, 20 to 40 µm thick sections were cut from perfused mouse brain on a vibratome (LEICA VT1200). Immunolabeling against aSyn pathology allowed for the identification of immuno-positive sections to be used for further processing with EM. For this, the sections were incubated overnight with a primary EP1536Y (Abcam) antibody at 4°C followed by Alexa-conjugated secondary antibody staining together with DAPI for cell nuclei identification. Fluorescence images were acquired with a Leica Thunder Tissue Imager equipped with a K8 fluorescent camera. Chosen sections with strong aSyn pathology were prepared for EM by post-fixing in reduced 2% osmium, thiocarbohydrazide and 2% Osmium tetroxide, followed by contrasting in 2% uranyl acetate and lead aspartate treatment at 60°C. The sections were dehydrated with an increasing acetone gradient, before infiltration with EMBED 812 resin for final flat embedding. The hardened sections were imaged again by light microscopy and the sections overlayed with the overview fluorescence map by using identifiable tissue features. Regions of interest were marked and the coordinates used for laser dissection. The resulting blocks were laser cut using a Leica LMD7 and glued onto a resin block. Serial sectioning with an ultra-microtome (Leica UC7) produced 120 to 200 nm thick tissue sections that were alternatingly collected on EM grids (slot and hexagonal grids) or glass slides. Glass slides were further processed for immunohistochemistry and toluidine blue staining.

Light microscopy images were acquired at 40x magnification and correlated to each other for the generation of an image overlay of pathology signal (IHC) and high contrast tissue morphology (toluidine blue). The resulting overlays were then correlated to low magnification (640x nominal magnification) EM overviews for cell identification by using identifiable tissue features both in the LM and EM images. The identified pathology was finally imaged and merged at high magnification in a tile acquisition series. For EM image acquisition, a Thermo Fisher Scientific (TFS) Talos F200C with a CETA camera or a CM100 (Phillips) with a TVIPS F416 camera were used. LM and EM images were adjusted for brightness and contrast where necessary.

Electron tomography and 3D reconstruction

Electron tomography data was collected using the Tomography software (TFS) with multi-site batch acquisition on a TFS Talos F200C with tilt series covering -60º to +60º in 2º steps. Tomograms were reconstructed using IMOD[56] and filtered with a non-local-means filter with Amira (TFS Amira version 2021.2). For segmentation, nuclear membranes, fibrils, and other membranous parts were manually annotated and traced throughout the tilt-series using Amira. Every few slices the respective feature of interest was selected by drawing directly onto the image and then interpolated to generate an accurate 3D volume. The final volume was visualised directly in AMIRA.

1.9 Cryo-electron microscopy

Cryo-EM grids were prepared using a Leica GP2 plunge freezer in a BSL-2 environment at room temperature. Quantifoil 2/1, 300 mesh, gold grids were glow discharged in air for 90s. Grids were prepared using 3 µl of 1:1 and 1:2 diluted fibril samples in preparation buffer (H2O, 100 mM NaCl, and 20 mM tris-HCl (pH 7.40)) and vitrification by rapid freezing in liquid ethane.

The grids were screened for fairly non-clustered fibers and high-resolution images were acquired with an automated EPU setup on a TFS Titan Krios G4 (TFS) electron microscope equipped with a cold-FEG 300kV electron source and a Falcon4i camera. The raw movies (EER) were collected with a total dose of 40 e-/Å^2 at a pixel spacing of 0.66 Å at the sample level. A defocus range between -0.8 µm and -1.8 µm was used during the acquisition.

Helical reconstruction and model building

All the subsequent image processing and helical reconstruction was carried out in RELION 4.0[57]. The recorded movies were gain corrected, motion corrected and dose weighted using RELION's own implementation of MOTIONCOR. The raw EER files were dose-fractionated to a total of 32 frames (1.23 e-/Å^2 per frame). After CTF estimation using Ctffind 4.1[58], the aligned averages that are better than the estimated CTF resolution of 5Å were selected resulting in a total of 11'879 micrographs. aSyn fibers were picked manually as start-to-end helical segments and extracted with an inter-box distance of 19 Å. Many rounds of reference-free 2D classification were performed to exclude suboptimal 2D segments from further processing. A very few best classes were selected and binned 4 times to re-extract the segments with a bigger box size encompassing the entire helical crossover. Clearly visible twisted class averages containing the entire crossover were used to generate initial de novo models using relion_helix_inimodel2d program. The most likely twist was estimated from a crossover distance measured from 2D class averages and corroborated with the direct measurements from micrographs.

The helical segments (105496) from the entire dataset were then re-extracted with 600 pix box size (binned by 2) comprising about 40 % of the crossover. Excluding the suboptimal classes after 2D classification resulted in 64889 particles. Multiple rounds of 3D auto-refinement were carried out to optimize the helical twist and rise, and also to check for the correct symmetry operators. This was validated from the reconstructions showing clear separation of beta-strands along the helical axis. Imposing a 2_1 cork-screw symmetry (pseudo two-fold symmetry) yielded the clear separation of beta-strands when compared to C1 and C2 symmetries. A 3D classification without image alignment was further performed to exclude the segments which gave suboptimal 3D volumes and resulted in final 51272 particles. These were finally re-extracted with 512 pix (unbinned) box size and underwent 3D auto-refine followed by CTF refinement. Further iterations of Bayesian Polishing coupled with CTF refinement yielded a high-resolution electron density map at 1.94 Å. The maps were sharpened using standard postprocessing procedure in RELION with an ad-hoc B-factor of 21 Å^2.

The atomic model for the backbone of the core of the 1B fibrils encompassing residues 34 to 95 was built de novo using Coot[59]. Initially three beta-rungs were modeled in coot and were refined in real-space in PHENIX[60]. Finally these chains were extended to 9 beta-rungs per protofilament and refined in tandem with phenix.real_space_refine and in coot to improve the Ramachandran and Geometric statistics. NCS and secondary structural restraints were included during the iterative refinement process.

On-grid immunogold labelling and analysis

EM grids with tissue sections were placed on a droplet of etching solution (1% periodic acid in water, Sigma Aldrich, United States), with the sections facing down, for 2.5 minutes. Grids were washed 3 times for 2 minutes in ddH_2O, then washed 2 times for 2 minutes in washing buffer (stock solution of 10% BSA, Aurion, which was 1/50 diluted in ddH_2O), and blocked in blocking solution (Aurion) for 5 minutes to reduce non-specific binding. Grids were then incubated with primary antibody (EP1526Y, Abcam, 1/50 diluted in washing buffer) for 60 minutes, washed 6 times for 2 minutes in blocking buffer, and then incubated in a solution of gold nanoparticles with a size of 10 nm (protein A gold, Aurion, 1/50 diluted in washing buffer) for 90 minutes. They were washed 3 times for 2 minutes in blocking solution, 3 times for 2 minutes in washing buffer, and 4 times for 1 minute in ddH_2O. Finally, grids were post-stained in 1% uranyl acetate for 1 minute and washed 3 times for 10 seconds in ddH_2O. Sections were imaged with a transmission electron microscope (TFS Talos L120C), operated at an operating voltage of 120 kV, and images were recorded with a TFS Ceta camera.

Gold particles were detected automatically in the recorded EM images, using FIJI[61], by applying a difference-of-gaussian filter (sigma1 = 10 nm, sigma2 = $\sqrt{2}$ • sigma1). The resulting image was binarized with a manually selected threshold. Particle detections with an area smaller than 25 nm^2 and a circularity (4π•area/perimeter^2) below 0.8 were excluded from analysis. The local density of gold was calculated as the decadic logarithm of the sum of a pixel's distance to the 15 closest neighboring gold particles. The gold particle detection was implemented as a FIJI macro and the density calculation as a python notebook.

Atomic force microscopy

1B aSyn fibrils were deposited on a freshly cleaved mica disk and left to adhere for 15 minutes in a humid chamber at room temperature. The sample was rinsed and imaged in saline buffer solution (H_2O, HEPES 20 mM, NaCl 100 mM, pH 7.4). AFM imaging was performed using the Dimension FastScan setup (Bruker) operating in PeakForce Quantitative Nano-Mechanics (PF-QNM) mode in liquid at room temperature, using sharp SNL-C probes (Bruker, Silicon tips on silicon nitride cantilevers), with a nominal spring constant of 0.24 N/m, a resonance frequency of 56 kHz, and a nominal tip radius of 2 nm. Fibrils were imaged with a peak force frequency of 1 kHz, a scan rate of 0.5 Hz and a constant setpoint force of 500 pN. Image analysis was performed using Nanoscope analysis (Bruker).

References

1. Poewe, W. *et al.* Multiple system atrophy. *Nat. Rev. Dis. Primer* **8**, 1–21 (2022).
2. Jellinger, K. A. Multiple System Atrophy: An oligodendroglioneural synucleinopathy. *J. Alzheimers Dis.* **62**, 1141–1179 (2018).
3. Dickson, D. W., Lin, W., Liu, W. K. & Yen, S. H. Multiple system atrophy: a sporadic synucleinopathy. *Brain Pathol.* **9**, 721–732 (1999).
4. Arima, K. *et al.* NACP/alpha-synuclein immunoreactivity in fibrillary components of neuronal and oligodendroglial cytoplasmic inclusions in the pontine nuclei in multiple system atrophy. *Acta Neuropathol. (Berl.)* **96**, 439–444 (1998).
5. Dickson, D. W. *et al.* Glial cytoplasmic inclusions (GCI) of multiple system atrophy (MSA) contain α-synuclein. *Mov. Disord.* **13**, 128 (1998).
6. Wakabayashi, K. *et al.* Accumulation of alpha-synuclein/NACP is a cytopathological feature common to Lewy body disease and multiple system atrophy. *Acta Neuropathol. (Berl.)* **96**, 445–452 (1998).
7. Tu, P. H. *et al.* Glial cytoplasmic inclusions in white matter oligodendrocytes of multiple system atrophy brains contain insoluble alpha-synuclein. *Ann. Neurol.* **44**, 415–422 (1998).
8. Gai, W. P., Power, J. H., Blumbergs, P. C. & Blessing, W. W. Multiple-system atrophy: a new alpha-synuclein disease? *Lancet Lond. Engl.* **352**, 547–548 (1998).
9. Watts, J. C. *et al.* Transmission of multiple system atrophy prions to transgenic mice. *Proc. Natl. Acad. Sci. U. S. A.* **110**, 19555–19560 (2013).
10. Prusiner, S. B. *et al.* Evidence for α-synuclein prions causing multiple system atrophy in humans with parkinsonism. *Proc. Natl. Acad. Sci. U. S. A.* **112**, E5308-5317 (2015).
11. Schweighauser, M. *et al.* Structures of α-synuclein filaments from multiple system atrophy. *Nature* **585**, 464–469 (2020).
12. Lövestam, S. *et al.* Seeded assembly in vitro does not replicate the structures of α-synuclein filaments from multiple system atrophy. *FEBS Open Bio* **11**, 999–1013 (2021).
13. De Giorgi, F. *et al.* Neurons with cat's eyes: A synthetic strain of α-synuclein fibrils seeding neuronal intranuclear inclusions. *Biomolecules* **12**, 436 (2022).
14. De Giorgi, F. *et al.* Novel self-replicating α-synuclein polymorphs that escape ThT monitoring can spontaneously emerge and acutely spread in neurons. *Sci. Adv.* **6**, eabc4364 (2020).
15. De Nuccio, F. *et al.* Oligodendrocytes prune axons containing α-synuclein aggregates in vivo: Lewy neurites as precursors of glial cytoplasmic inclusions in Multiple System Atrophy? *Biomolecules* **13**, 269 (2023).
16. Tao, Y. *et al.* Structural mechanism for specific binding of chemical compounds to amyloid fibrils. *Nat. Chem. Biol.* **19**, 1235–1245 (2023).
17. Papp, M. I., Kahn, J. E. & Lantos, P. L. Glial cytoplasmic inclusions in the CNS of patients with multiple system atrophy (striatonigral degeneration, olivopontocerebellar atrophy and Shy-Drager syndrome). *J. Neurol. Sci.* **94**, 79–100 (1989).
18. Kato, S. *et al.* Argyrophilic ubiquitinated cytoplasmic inclusions of Leu-7-positive glial cells in olivopontocerebellar atrophy (multiple system atrophy). *Acta Neuropathol. (Berl.)* **82**, 488–493 (1991).

19. Papp, M. I. & Lantos, P. L. Accumulation of tubular structures in oligodendroglial and neuronal cells as the basic alteration in multiple system atrophy. *J. Neurol. Sci.* **107**, 172–182 (1992).

20. Spillantini, M. G. *et al.* Filamentous alpha-synuclein inclusions link multiple system atrophy with Parkinson's disease and dementia with Lewy bodies. *Neurosci. Lett.* **251**, 205–208 (1998).

21. Gai, W. P., Power, J. H., Blumbergs, P. C., Culvenor, J. G. & Jensen, P. H. Alpha-synuclein immunoisolation of glial inclusions from multiple system atrophy brain tissue reveals multiprotein components. *J. Neurochem.* **73**, 2093–2100 (1999).

22. Peelaerts, W. *et al.* alpha-Synuclein strains cause distinct synucleinopathies after local and systemic administration. *Nature* **522**, 340–4 (2015).

23. Uemura, N. *et al.* Slow progressive accumulation of oligodendroglial alpha-synuclein (α-Syn) pathology in synthetic α-Syn fibril-induced mouse models of synucleinopathy. *J. Neuropathol. Exp. Neurol.* **78**, 877–890 (2019).

24. Bousset, L. *et al.* Structural and functional characterization of two alpha-synuclein strains. *Nat Commun* **4**, 2575 (2013).

25. Luk, K. C. *et al.* Molecular and biological compatibility with host alpha-synuclein influences fibril pathogenicity. *Cell Rep.* **16**, 3373–3387 (2016).

26. Shahnawaz, M. *et al.* Discriminating α-synuclein strains in Parkinson's disease and multiple system atrophy. *Nature* **578**, 273–277 (2020).

27. Guerrero-Ferreira, R. *et al.* Cryo-EM structure of alpha-synuclein fibrils. *eLife* **7**, e36402 (2018).

28. Li, B. *et al.* Cryo-EM of full-length α-synuclein reveals fibril polymorphs with a common structural kernel. *Nat. Commun.* **9**, 3609 (2018).

29. Lin, W.-L., DeLucia, M. W. & Dickson, D. W. α-Synuclein immunoreactivity in neuronal nuclear inclusions and neurites in multiple system atrophy. *Neurosci. Lett.* **354**, 99–102 (2004).

30. Nishie, M., Mori, F., Yoshimoto, M., Takahashi, H. & Wakabayashi, K. A quantitative investigation of neuronal cytoplasmic and intranuclear inclusions in the pontine and inferior olivary nuclei in multiple system atrophy. *Neuropathol. Appl. Neurobiol.* **30**, 546–554 (2004).

31. Woulfe, J. M. Abnormalities of the nucleus and nuclear inclusions in neurodegenerative disease: a work in progress. *Neuropathol. Appl. Neurobiol.* **33**, 2–42 (2007).

32. Hass, E. W. *et al.* Robust α-synuclein pathology in select brainstem neuronal populations is a potential instigator of multiple system atrophy. *Acta Neuropathol. Commun.* **9**, 80 (2021).

33. Laferrière, F., Claverol, S., Bezard, E., De Giorgi, F. & Ichas, F. Similar neuronal imprint and no cross-seeded fibrils in α-synuclein aggregates from MSA and Parkinson's disease. *NPJ Park. Dis.* **8**, 10 (2022).

34. Boyer, D. R. *et al.* Structures of fibrils formed by α-synuclein hereditary disease mutant H50Q reveal new polymorphs. *Nat. Struct. Mol. Biol.* **26**, 1044–1052 (2019).

35. Pesch, V. *et al.* Vaccination with structurally adapted fungal protein fibrils induces immunity to Parkinson's disease. *Brain* awae061 (2024) doi:10.1093/brain/awae061.

36. Beton, J. G. *et al.* Cooperative amyloid fibre binding and disassembly by the Hsp70 disaggregase. *EMBO J.* **41**, e110410 (2022).

37. Shahmoradian, S. H. *et al.* Lewy pathology in Parkinson's disease consists of crowded organelles and lipid membranes. *Nat. Neurosci.* **22**, 1099–1109 (2019).

38. St-Pierre, M.-K. *et al.* Ultrastructural characterization of dark microglia during aging in a mouse model of Alzheimer's disease pathology and in human post-mortem brain samples. *J. Neuroinflammation* **19**, 235 (2022).

39. Tremblay, M.-È. Microglial functional alteration and increased diversity in the challenged brain: Insights into novel targets for intervention. *Brain Behav. Immun. - Health* **16**, 100301 (2021).

40. Böing, C. *et al.* Distinct ultrastructural phenotypes of glial and neuronal alpha-synuclein inclusions in multiple system atrophy. *Brain* awae137 (2024) doi:10.1093/brain/awae137.

41. Guerrero-Ferreira, R., Kovacik, L., Ni, D. & Stahlberg, H. New insights on the structure of alpha-synuclein fibrils using cryo-electron microscopy. *Curr. Opin. Neurobiol.* **61**, 89–95 (2020).

42. Sun, Y. *et al.* Cryo-EM structure of full-length α-synuclein amyloid fibril with Parkinson's disease familial A53T mutation. *Cell Res.* **30**, 360–362 (2020).

43. Seidel, K. *et al.* First appraisal of brain pathology owing to A30P mutant alpha-synuclein. *Ann. Neurol.* **67**, 684–689 (2010).

44. Nishioka, K. *et al.* Pathological findings in a patient with alpha-synuclein p.A53T and familial Parkinson's disease. *Parkinsonism Relat. Disord.* **81**, 183–187 (2020).

45. Pasanen, P. *et al.* Novel α-synuclein mutation A53E associated with atypical multiple system atrophy and Parkinson's disease-type pathology. *Neurobiol. Aging* **35**, 2180.e1–5 (2014).

46. Kiely, A. P. *et al.* Distinct clinical and neuropathological features of G51D SNCA mutation cases compared with SNCA duplication and H50Q mutation. *Mol. Neurodegener.* **10**, 41 (2015).

47. Sun, C. *et al.* Cryo-EM structure of amyloid fibril formed by α-synuclein hereditary A53E mutation reveals a distinct protofilament interface. *J. Biol. Chem.* **299**, 104566 (2023).

48. Sun, Y. *et al.* The hereditary mutation G51D unlocks a distinct fibril strain transmissible to wild-type α-synuclein. *Nat. Commun.* **12**, 6252 (2021).

49. Woerman, A. L. *et al.* Familial Parkinson's point mutation abolishes multiple system atrophy prion replication. *Proc. Natl. Acad. Sci. U. S. A.* **115**, 409–414 (2018).

50. Holec, S. A. M. *et al.* The E46K mutation modulates α-synuclein prion replication in transgenic mice. *PLoS Pathog.* **18**, e1010956 (2022).

51. Sargent, D. *et al.* 'Prion-like' propagation of the synucleinopathy of M83 transgenic mice depends on the mouse genotype and type of inoculum. *J. Neurochem.* **143**, 126–135 (2017).

52. Balana, A. T. *et al.* O-GlcNAc forces an α-synuclein amyloid strain with notably diminished seeding and pathology. *Nat. Chem. Biol.* (2024) doi:10.1038/s41589-024-01551-2.

53. Oueslati, A., Paleologou, K. E., Schneider, B. L., Aebischer, P. & Lashuel, H. A. Mimicking phosphorylation at serine 87 inhibits the aggregation of human α-synuclein and protects against its toxicity in a rat model of Parkinson's disease. *J. Neurosci. Off. J. Soc. Neurosci.* **32**, 1536–1544 (2012).

54. Paleologou, K. E. *et al.* Phosphorylation at Ser-129 but not the phosphomimics S129E/D inhibits the fibrillation of alpha-synuclein. *J. Biol. Chem.* **283**, 16895–16905 (2008).

55. de Chaumont, F. *et al.* Icy: an open bioimage informatics platform for extended reproducible research. *Nat. Methods* **9**, 690–696 (2012).

56. Kremer, J. R., Mastronarde, D. N. & McIntosh, J. R. Computer visualization of three-dimensional image data using IMOD. *J. Struct. Biol.* **116**, 71–6 (1996).

57. Kimanius, D., Dong, L., Sharov, G., Nakane, T. & Scheres, S. H. W. New tools for automated cryo-EM single-particle analysis in RELION-4.0. *Biochem. J.* **478**, 4169–4185 (2021).

58. Rohou, A. & Grigorieff, N. CTFFIND4: Fast and accurate defocus estimation from electron micrographs. *J. Struct. Biol.* **192**, 216–221 (2015).

59. Emsley, P. & Cowtan, K. Coot: model-building tools for molecular graphics. *Acta Crystallogr. D Biol. Crystallogr.* **60**, 2126–32 (2004).

60. Afonine, P. V. *et al.* Real-space refinement in PHENIX for cryo-EM and crystallography. *Acta Crystallogr Struct Biol* **74**, 531–544 (2018).

61. Schindelin, J. *et al.* Fiji: an open-source platform for biological-image analysis. *Nat. Methods* **9**, 676–682 (2012).

Acknowledgements

Cryo-EM data were in part collected at the Dubochet Center for Imaging (DCI) in Lausanne. The DCI-Lausanne is a joint initiative of the EPFL and the Universities of Lausanne and Geneva. We thank Alex Myasnikov from the DCI-Lausanne for expert technical assistance in cryo-EM data collection, Marie-Hélène Canron and Francesca Serinelli for support with paraffin histology, Sandra Dovero and Nathalie Biendon for support with Pannoramic™ slide scanning, Benjamin Dehay for sharing the AAV-Syn mutants vectors, Marion Picquemal for support with animal surgery, Sabrina Lacomme and Fabrice Cordelières from the Bordeaux Imaging Center for their help with sample fixation for CLEM and with the Zeiss CD7 platform respectively. Room-temperature EM was collected in part at the electron microscopy facility (EMF) of the University of Lausanne. We thank Christel Genoud and the whole EMF team for their assistance throughout the project.

Author contributions

FI and HS conceived and managed the project. FI, HS, FDG, DDL and TB designed the experiments. DB, FI and HS wrote the first version of the manuscript. DB and IM performed the sample preparation and image acquisition for cryo-EM. DB performed the structural analysis. MK and FDN performed in vivo experiments in wild-type mice and neuropathology stainings. DB and AJL performed the CLEM experiments. DB and LvdH performed the immunogold labelling, and LvdH the immunogold analysis. HdLS, FDG and FI produced aSyn and fingerprinted 1B. JV performed the in vivo experiments in transgenic M83 mice. CF performed the AFM of 1B fibrils. HdLS, MB and AL SEC-purified aSyn. MLA, AR and EB performed in vivo experiments in wild-type mice. FL and LB participated in early characterizations of 1B. FDG and FI performed the HCA experiments, as well as the confocal and slide scanning neuropathology analyses of wild-type and M83 mice. All authors contributed to the writing of the manuscript.

Data availability

Raw cryo-EM images are available at the EMPIAR database, accession number EMPIAR-12012. The reconstructed 3D map is available at the EMDB database, accession number EMD-19986. The atomic model is available at the PDB database, accession number PDB-9EUU.

Funding

This work was supported by the Swiss National Science Foundation, Grant 310030_188548, the Swiss Parkinson Foundation, the Department of Excellence Initiative of the Italian Ministry of Research, and the French Agence Nationale de la Recherche, Grant ANR-22-CE16-0002.

Ethical compliance

All experimental procedures were conducted in accordance with the European Communities Council Directive (2010/63/EU) for care of laboratory animals. The animal study protocol was approved by the animal experimentation ethics committee of the University of Bordeaux, and validated by the French Ministry of Research (protocol APAFIS #33147-2021091711598830 v6, 2021–2026).

Competing interests

The authors declare no competing interests.

Extended data figures

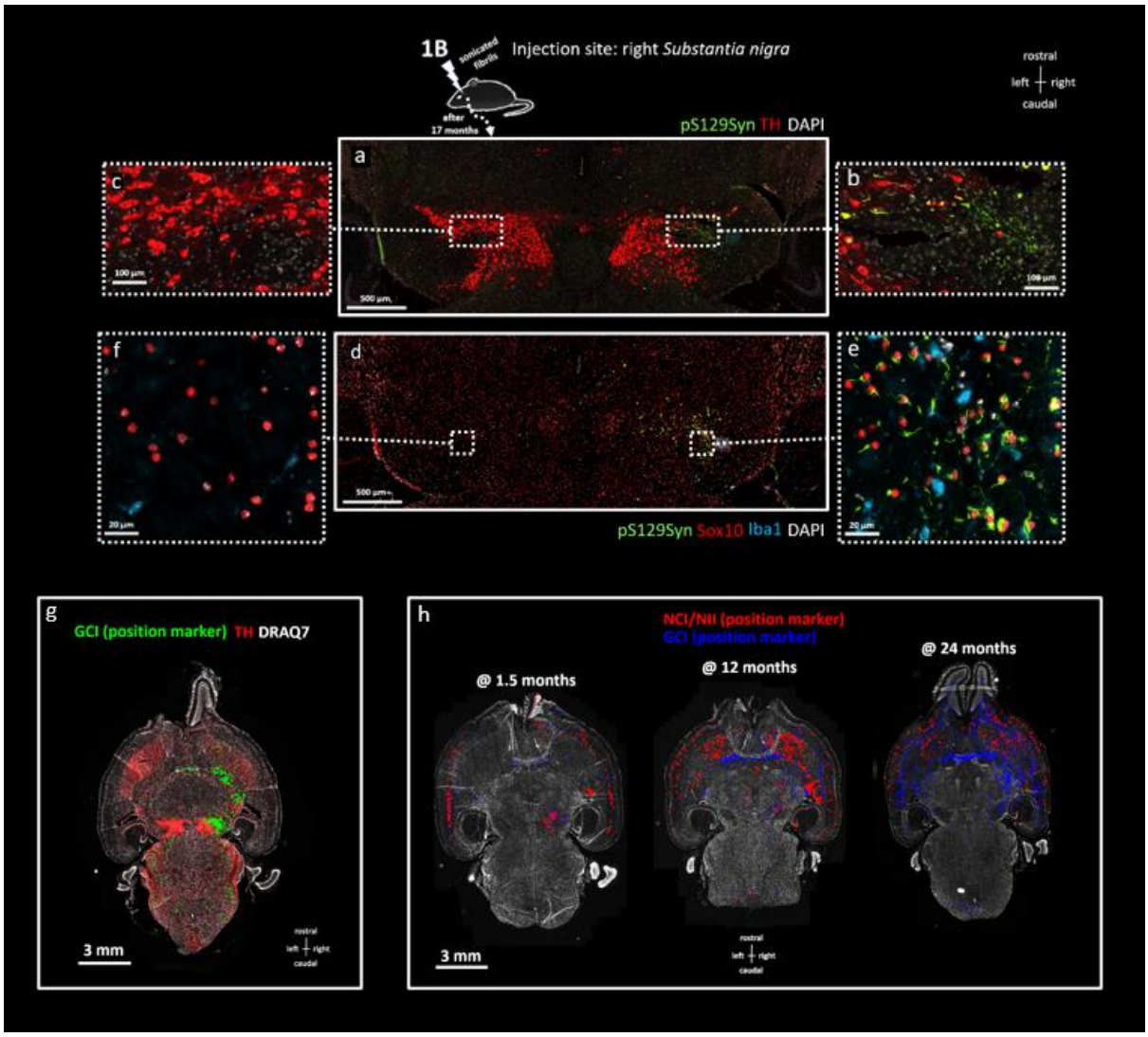

Extended Data Fig. 1 | Semi-topographic view of a horizontal brain section from a wild-type mouse injected 17 months earlier at the level of its right substantia nigra (SN) with 1B fibrils *(For red-green color-blind readers, see alternative color version in supp. data section).* ***a.*** *aSyn inclusions are revealed using the anti-phospho aSyn antibody #64 (green), dopaminergic neurons using an anti-tyrosine hydroxylase antibody (TH, red) and nuclei using DAPI (white). Left and right SNs are visible with a loss of symmetry of the right SN with depletion of TH-positive neurons and unilateral aSyn inclusions. The TH-depleted/aSyn inclusion-rich region is enlarged in* ***b****, the corresponding left region is enlarged in* ***c****.* ***d.*** *Semi-topographic view of the n+1 horizontal section consecutive to (a). aSyn inclusions in green (anti-phospho aSyn antibody #64), OLs in red (anti-Sox10 antibody), microglial cells in blue (anti -Iba1) and nuclei in white (DAPI). The right SN enlarged in* ***e*** *contains numerous GCIs and sparse microglial cells.* ***f*** *Enlarged view of the corresponding region of the left SN.* ***g.*** *anatomical distribution of CGIs in the brain of the mouse shown in (a). Full brain horizontal section view. GCI positions: green dots, TH: red, DAPI: white.* ***h.*** *Anatomical distribution of NCIs and NIIs (red) and CGIs (blue) (Lewy neurites not annotated) in the brains of mice sacrificed 1.5, 12, and 24 months after injection of 1B fibrils in their right caudate putamen. Same horizontal sections as the ones shown in* ***Fig. 1f*** *but with NCI/NII annotated. Scale bars: a, d = 500 µm; b, c = 100µm; e, f = 20 µm; g, h = 3 mm.*

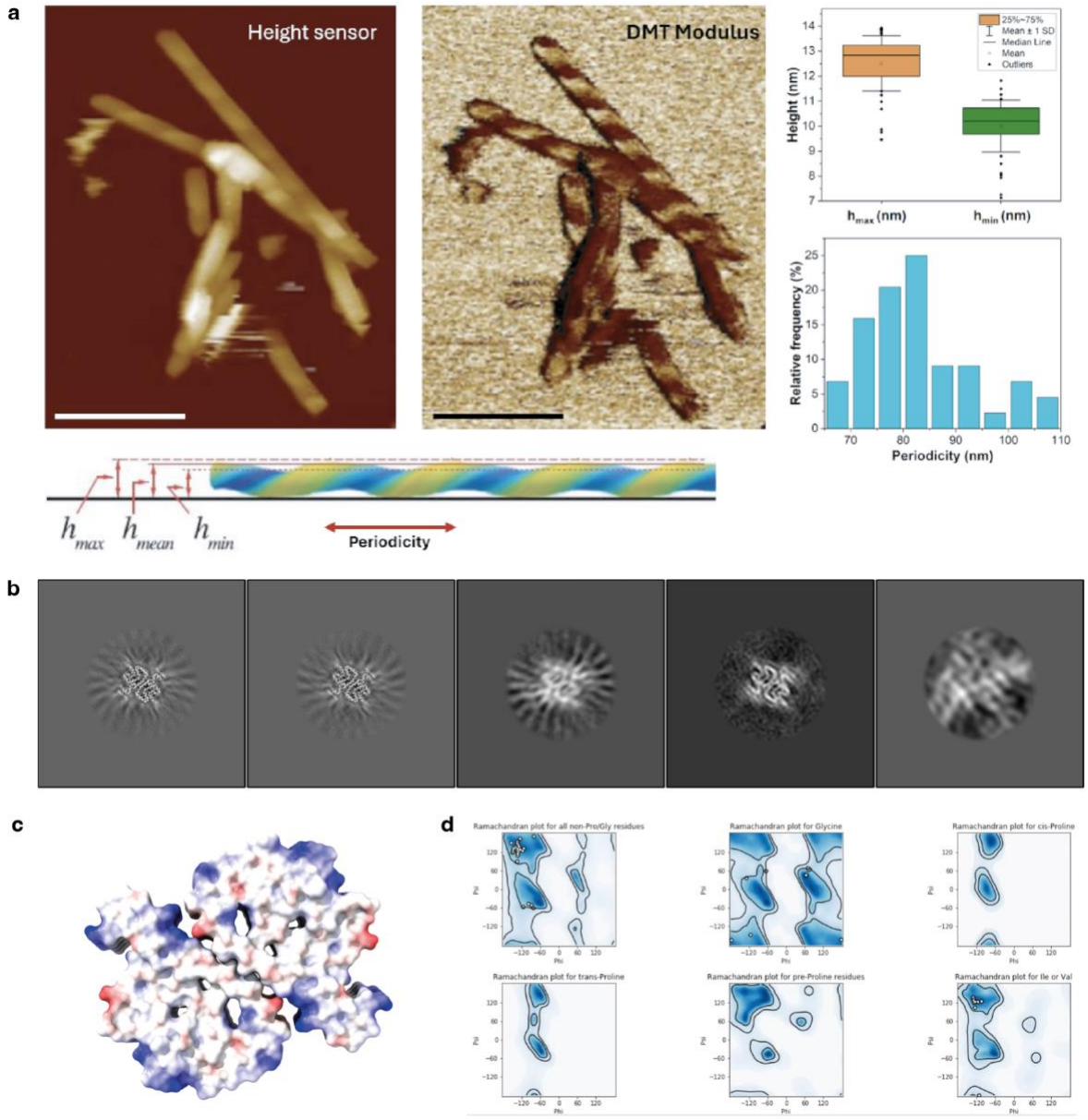

Extended Data Fig. 2 | Structural validation of 1B fibrils. a. *Topographical (Height Sensor) and nano-mechanical mapping (Derjaguin-Müller-Toporov (DMT) Modulus) of 1B fibrils using atomic force microscopy (AFM) in liquid. Right panels: fibril height values (see cartoon for definitions) for n = 103 measurements, and left twist periodicity for n = 12 fibrils. Scale bars = 240 nm.* ***b****. Cross-sections of 3D classification results of EM images, indicating the presence of only 1 polymorph in the entire dataset. The class averages 1, 2 and 4 from the left combine to a total of approx. 60,000 particles. The particles from classes 3 and 5 were discarded.* ***c.*** *Electropotential map of the 3D reconstruction from cryo-EM, encompassing residues 34 to 95. Blue: positive charges. Res: negative charges.* ***d.*** *Ramachandran plot for the determined 1B model for residues 34 to 95, indicating 96.61% favored, 3.39% allowed, and 0.00% outliers.*

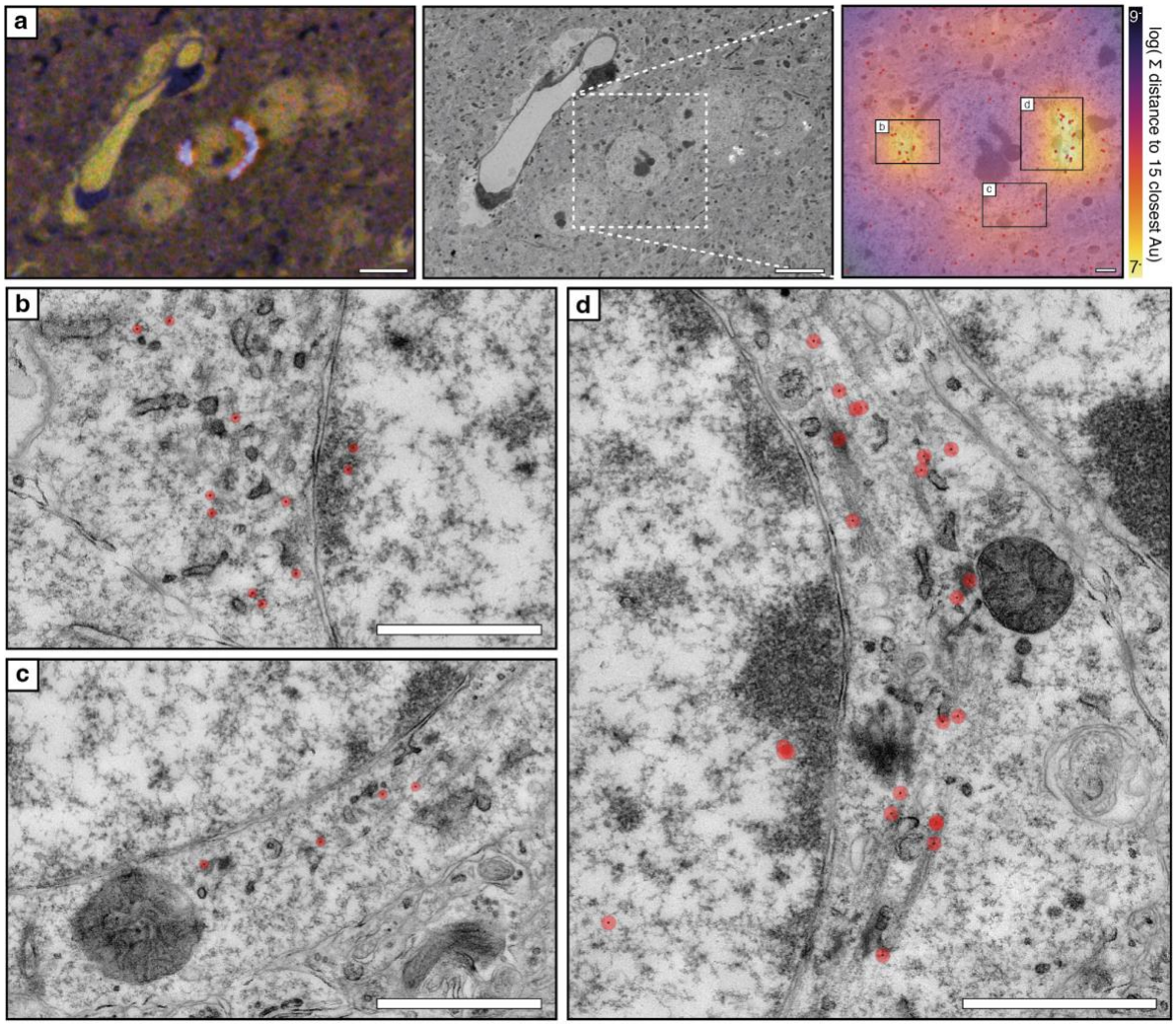

Extended Data Fig. 3 | Immunogold analysis against aSyn in the mouse brain. a. *Immunohistochemistry (IHC) labelling indicates two regions with aSyn pathology wrapping around the nucleus of an affected cell. The correlated EM image with on-grid immunolabelling against aSyn shows an increase of gold particles in comparison to the background as indicated by the heatmap. Higher magnifications are indicated by the labelled boxes.* ***b.*** *Zoomed view on the left side of the nucleus, highlighted are the gold particles in red, laying on top of dispersed fibrils.* ***c.*** *Lower part of the pathology from the right side of the cell. The zoomed area shows four gold particles laying on top of fibril pathology.* ***d.*** *Zoom of right-side pathology, with highest concentration of gold particles, laying on fibril bundles. Scale bars = 5 µm for overlay and low magnification EM, 1 µm for heatmap and zoomed EM views.*

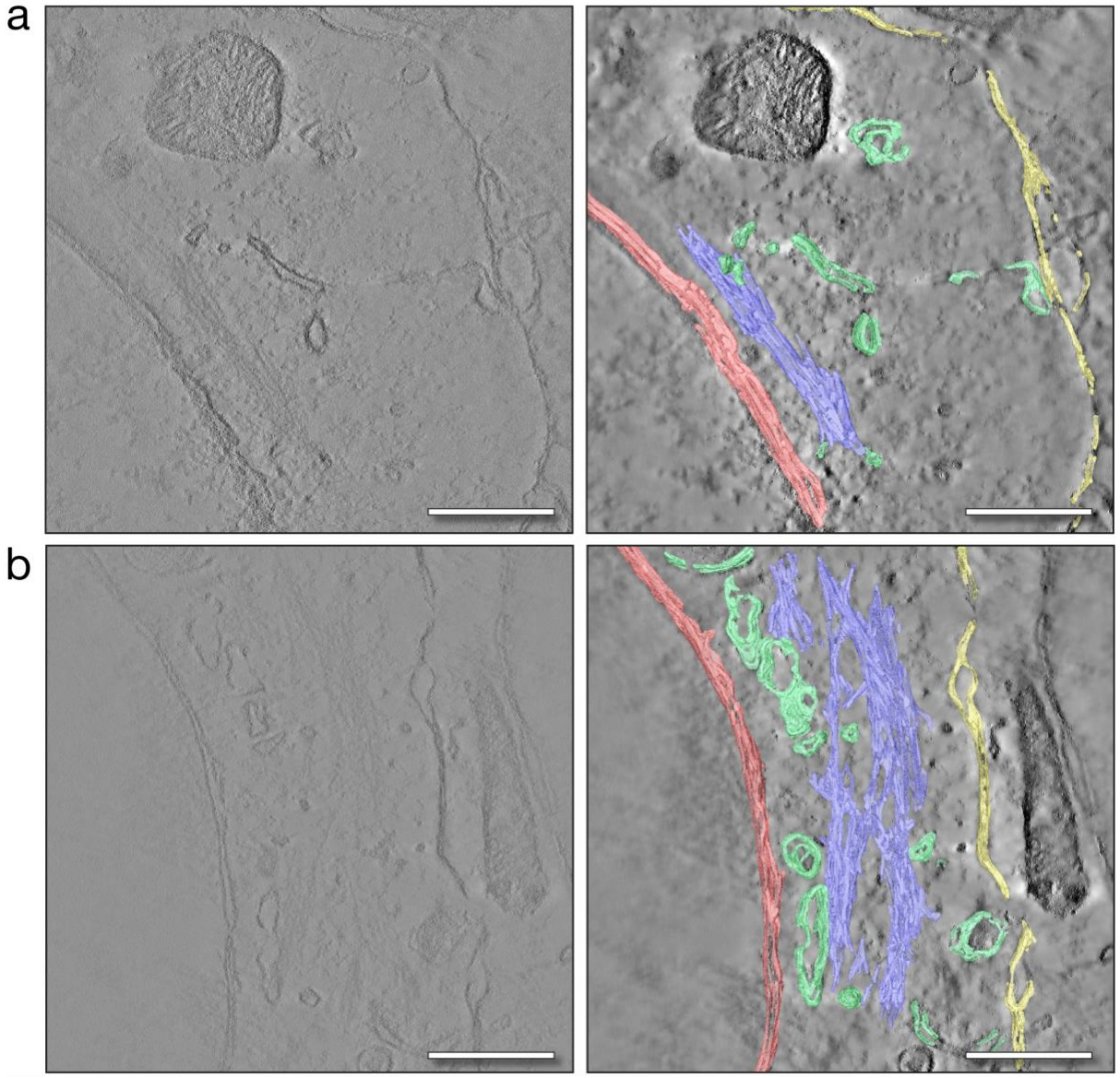

Extended Data Fig. 4 | Tomogram segmentation of aSyn fibril bundles. *Tomograms were manually segmented to visualise the fibril bundling (blue), the nuclear membrane (red), the cell membrane (yellow), and other membranous compartments (green). Left: Central section of a tomogram. Right: Overlay with 3D-segmented elements.* ***a.*** *A GCI with a smaller, but dense fibril bundle.* ***b.*** *A GCI with a more loosely arranged fibril bundle, following along the nuclear curvature. Scale bars = 500 nm.*

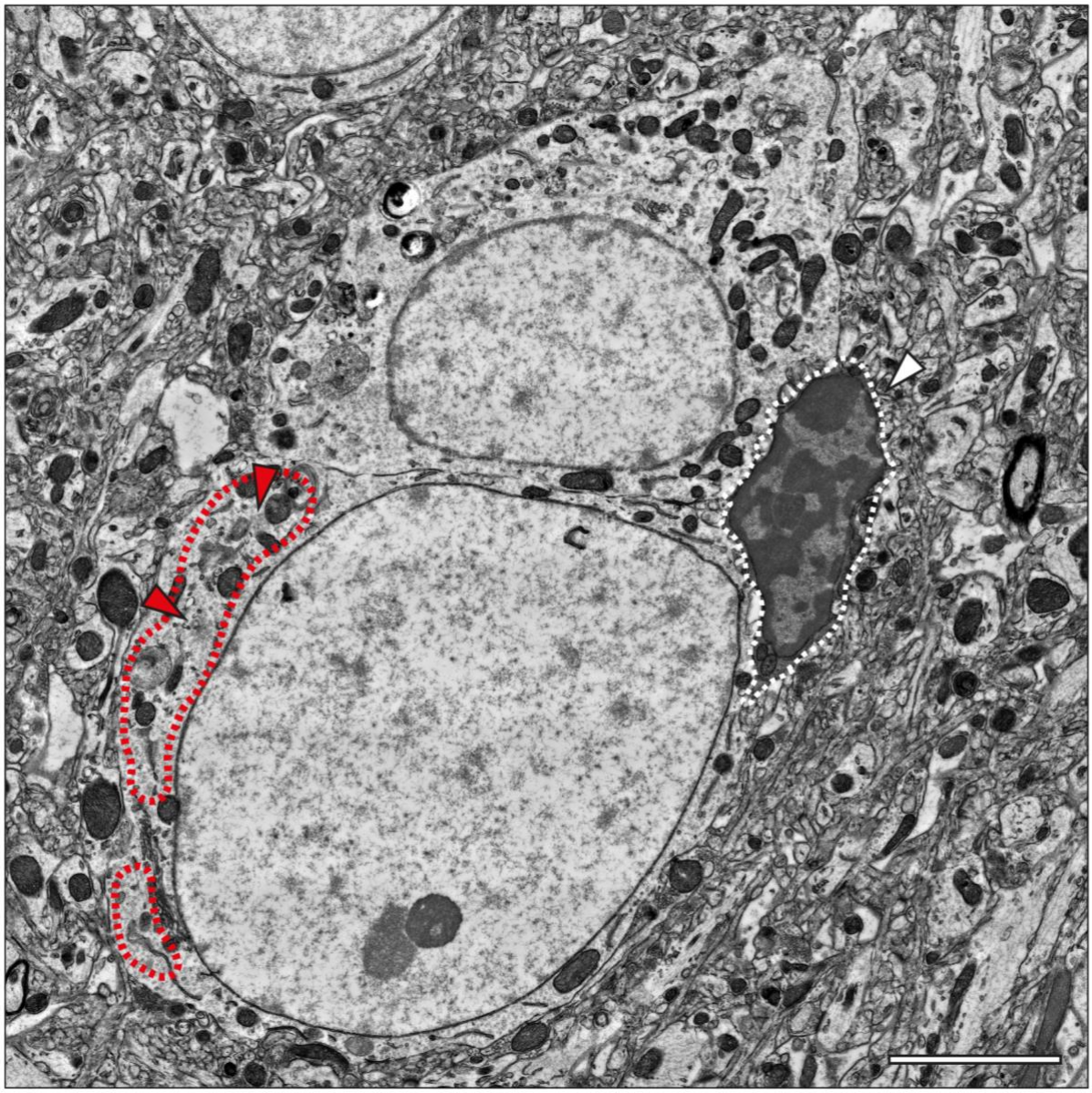

Extended Data Fig. 5 | Pathological oligodendrocyte in direct contact with other cells. *Cells with a distinct morphology, previously described as "dark microglia", can be found in close proximity or in direct contact with pathological cells (white arrowhead). The total cell volume of the dark microglia is indicated by the white dashed line. In this specific case the fibrillar pathology of the oligodendrocyte appears in a dispersed arrangement with two smaller clusters (red arrowheads). Total area of immunopositive IHC is indicated by a red dashed line. Both oligodendrocytes contain aSyn pathology however for the upper cell volume it is not visible in this EM slice (based on IHC positive signal from other EM grids). Scale bar = 3 µm.*

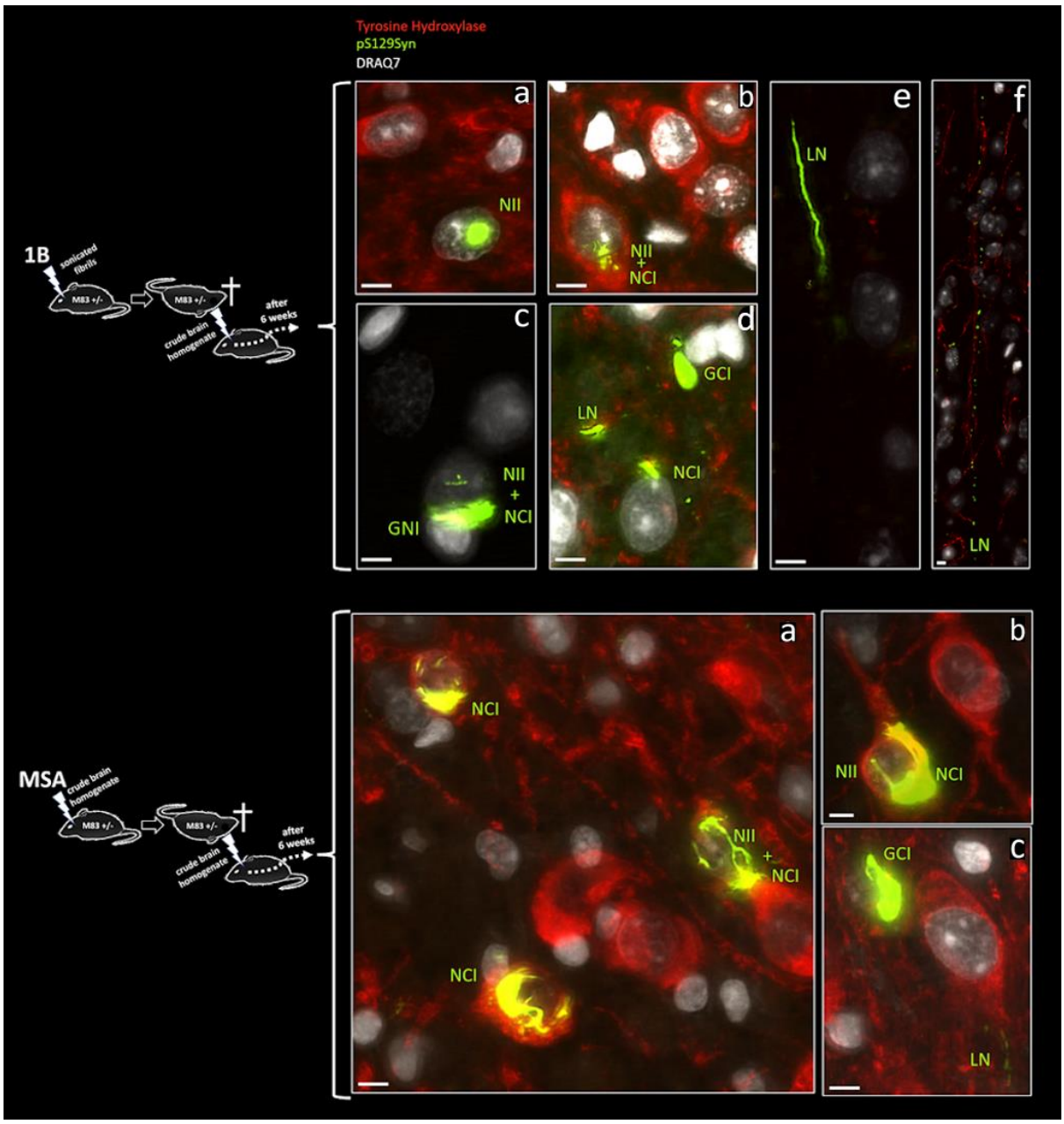

Extended Data Fig. 6 | Animal-to-animal transmission of aSyn pathology *(version for red-green color-blind readers available in supp. data section).* ***1B transmission panels:*** *examples of aSyn inclusions detected 6 weeks after crude brain homogenate inoculation in a wild-type mouse. NII: neuronal intranuclear inclusion; NCI: neuronal cytoplasmic inclusion; GNI: glial nuclear inclusion; LN: Lewy neurite; GCI: glial cytoplasmic inclusion.* ***a, b,*** *and* ***d*** *are from the right SNpc,* ***c, e*** *and* ***f*** *are from cortical regions.* ***MSA transmission panels:*** *examples of aSyn inclusions detected 6 weeks after crude brain homogenate inoculation in a wild-type mouse. Abbreviations are the same as in before.* ***a, b*** *and* ***c*** *are from the right SNpc. Scale bars = 5 µm. See corresponding 3D reconstructions and animations in Supplementary materials.*

Supplementary information

Confocal animations/3D reconstructions:

Movie-1: Section hovering overview corresponding to Fig1a-f: DAPI in blue, pS129Syn in white, Sox10 in pink, Iba1 in yellow (only in AC) Fig1a ACPL and BNST GCIs.mp4

Movie-2: 3D animation of NII & NCI shown in Extended Data Fig. 6. "1B transmission" panel **b**: DAPI in white, pS129Syn in green, Tyrosine Hydroxylase in red LeSTRIAP7 99c.mp4

Movie-3: 3D animation of NII shown in Extended Data Fig. 6. "1B transmission" panel **a**: DAPI in white, pS129Syn in green, Tyrosine Hydroxylase in red LeSTRIAP7 85.mp4

Movie-4: 3D animation of a Tyrosine Hydroxylase (red) positive cell from the s*ubstantia nigra* of the mouse sampled in Extended Data Fig. 6. "1B transmission". pS129Syn is in green. Both NCIs and NIIs can be observed without need for a nuclear marker LeSTRIAP7 97.mp4

Movie-5: 3D animation of Extended Data Fig. 6. "MSA transmission" panel **b,** showing the NII thread and the NCI in a TH-positive neuron: DAPI in white, pS129Syn in green, Tyrosine Hydroxylase in red LeSTRDS20 99.mp4

Movie-6: Zoomed view of 3D animation of Extended Data Fig. 6. "MSA transmission" panel **b** showing the NII thread and the NCI in a TH-positive neuron: DAPI in white, pS129Syn in green, Tyrosine Hydroxylase in red LeSTRDS20 99b.mp4

Movie-7: 3D animation of Extended Data Fig. 6. "1B transmission" panel **c**: The NCI of the cortical neuron (bigger nucleus) seems to protrude within the interior of the lining glial cell (smaller nucleus): DAPI in white, pS129Syn in green, Tyrosine Hydroxylase in red (not expressed in this region) LeSTRIAP7 99a.mp4

Movie-8: "in silico" section of 3D animation of Extended Data Fig. 6. "1B transmission" panel **c**: The NCI is in continuity with a glial nuclear inclusion (GNI): DAPI in white, pS129Syn in green, Tyrosine Hydroxylase in red (not expressed in this region) LeSTRIAP7 99b.mp4

Figures for readers with red-green color-blindness

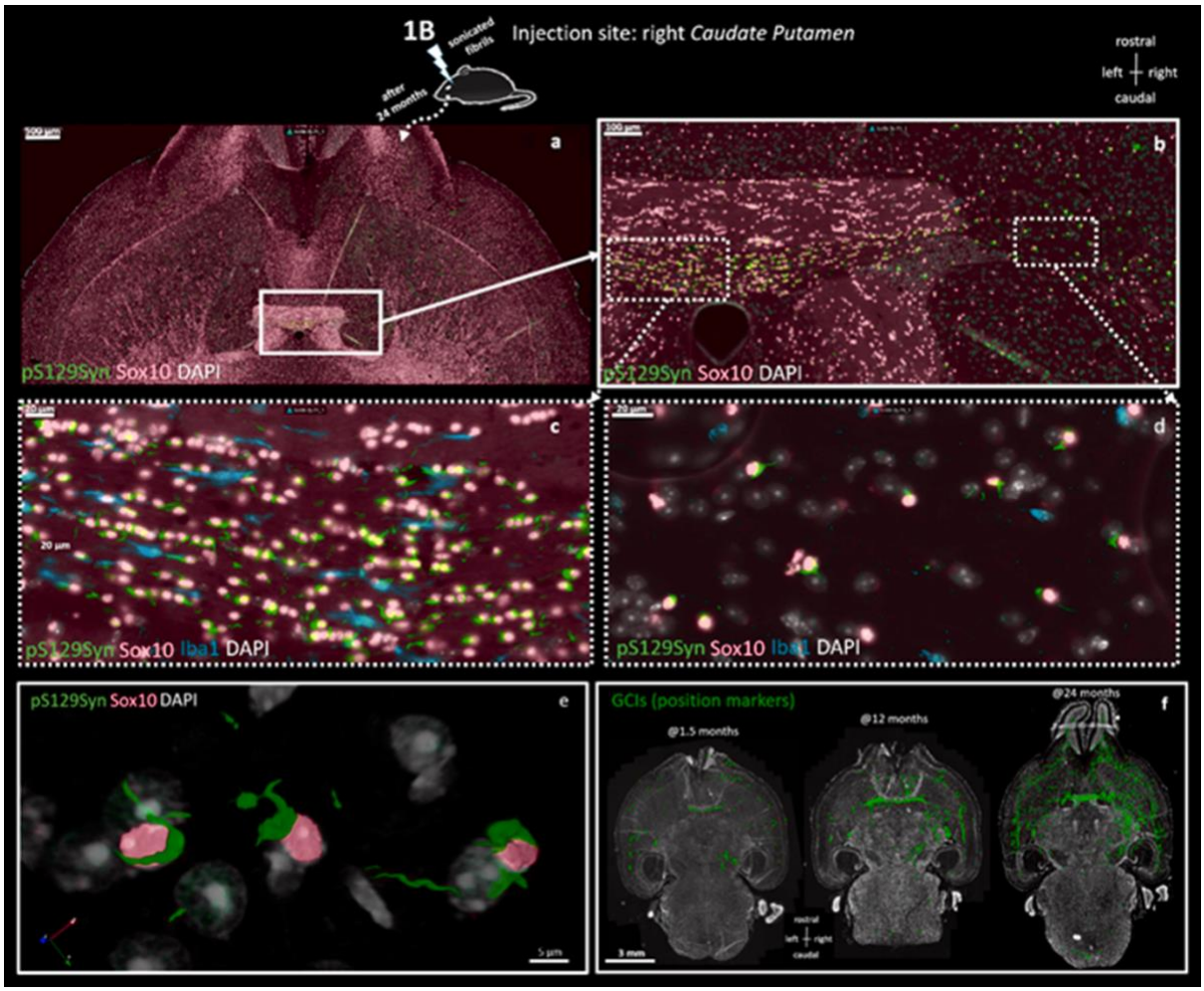

Color-blind version of Fig. 1 *(generated using the software Visolve Deflector 4.5)* | ***Seeding of GCIs in wild-type mice by alpha-synuclein fibrils from the 1B strain***. ***a.*** *topographic immuno-fluorescence view of a horizontal brain section from a wild-type mouse injected 24 months earlier at the level of its right CP with 1B fibrils. aSyn inclusions are revealed using the anti-phospho aSyn antibody #64 (green), OLs by an antibody against the OL nuclear marker Sox10 (red), and nuclei using DAPI (white). The sectional plane intercepts horizontally the AC and the BNST (plain box)* ***b.*** *Higher magnification of the latter box evidencing the specific invasion by aSyn inclusions of the posterior limb of the AC (left dashed box), and of the BNST (right dashed box).* ***c.*** *Higher magnification of the left dashed box in (b): interfascicular OLs populating the posterior limb of the AC bear aSyn inclusions, i.e., GCIs, and sparse microglial cells are revealed using an antibody against Iba1 (blue).* ***d.*** *Higher magnification of the right dashed box in (b): satellite Sox10-positive OLs populating the BNST bear aSyn inclusions, i.e., GCIs, and sparse Iba1-positive microglial cells are detectable.* ***e.*** *Bird's eye view of a confocal 3D volume reconstruction centred on 3 OLs of the BNST bearing GCIs, from the section shown in (a). See also* ***Supplementary data movie 1***. ***f.*** *Neuroanatomical distribution of GCIs in the brain of mice at 12 and 24 months post-1B injection in their right CP. Full brain horizontal sections. The 24 month section is the n+1 section adjacent to the one shown in (a). Scale bars: in a = 500 µm; in b = 100 µm; in c, d = 20 µm; in e = 5 µm; in f = 3 mm.*

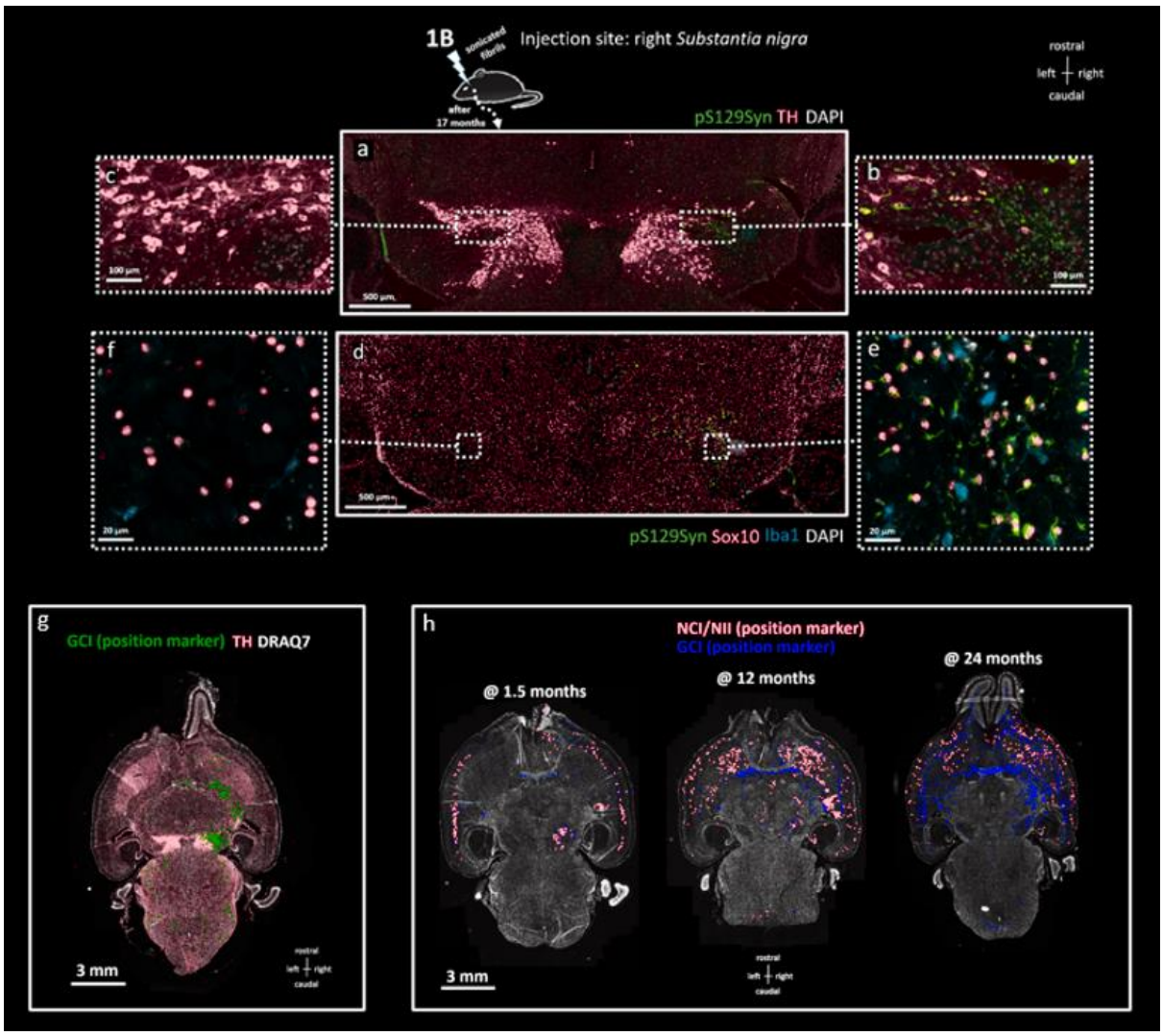

Color-blind version of Extended Data Fig. 1 *(generated using the software Visolve Deflector 4.5)* | ***Semi-topographic view of a horizontal brain section from a wild-type mouse injected 17 months earlier at the level of its right substantia nigra (SN) with 1B fibrils. a.*** *aSyn inclusions are revealed using the anti-phospho aSyn antibody #64 (green), dopaminergic neurons using an anti-tyrosine hydroxylase antibody (TH, red) and nuclei using DAPI (white). Left and right SNs are visible with a loss of symmetry of the right SN with depletion of TH-positive neurons and unilateral aSyn inclusions. The TH-depleted/aSyn inclusion-rich region is enlarged in* ***b****, the corresponding left region is enlarged in* ***c****.* ***d.*** *Semi-topographic view of the n+1 horizontal section consecutive to (a). aSyn inclusions in green (anti-phospho aSyn antibody #64), OLs in red (anti-Sox10 antibody), microglial cells in blue (anti -Iba1) and nuclei in white (DAPI). The right SN enlarged in* ***e*** *contains numerous GCIs and sparse microglial cells.* ***f*** *Enlarged view of the corresponding region of the left SN.* ***g.*** *anatomical distribution of CGIs in the brain of the mouse shown in (a). Full brain horizontal section view. GCI positions: green dots, TH: red, DAPI: white.* ***h.*** *Anatomical distribution of NCIs and NIIs (red) and CGIs (blue) (Lewy neurites not annotated) in the brains of mice sacrificed 1.5, 12, and 24 months after injection of 1B fibrils in their right caudate putamen. Same horizontal sections as the ones shown in* ***Fig. 1f*** *but with NCI/NII annotated. Scale bars: a, d = 500 µm; b, c = 100µm; e, f = 20 µm; g, h = 3 mm.*

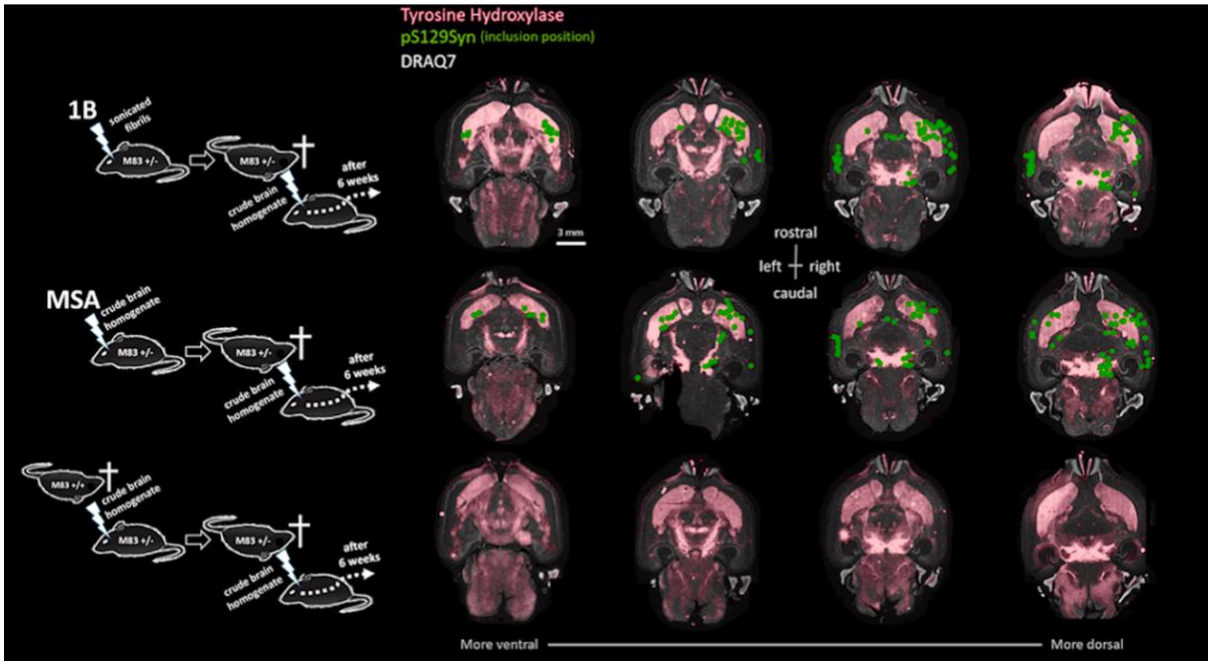

Color-blind version of Fig. 6 *(generated using the software Visolve Deflector 4.5)* | ***Animal-to-animal transmission of 1B and MSA aSyn pathology by crude brain homogenates.*** *Diluted crude brain homogenates were prepared from prematurely dying M83+/- mice that had been previously injected either with human 1B fibrils (upper row), or with a brain homogenate from a deceased MSA patient[51] (middle row), or with a brain homogenate from a spontaneously dying homozygous M83+/+ transgenic mouse (bottom row). The corresponding brain homogenates were injected in the right caudate putamen of 6 wild-type mice (2 per group). After 6 weeks, wild-type mice were sacrificed, and their brains were processed for horizontal sectioning and immunofluorescence neuropathology. aSyn inclusions were revealed using an anti-phospho aSyn antibody (EP1536Y, green), the nigrostriatal tract was evidenced using an anti-Tyrosine Hydroxylase antibody (TH, red) and the nuclei were revealed with DRAQ7 (white). 3 animals are displayed with 4 sections for each, sampling the nigrostriatal tract along its dorso-ventral axis. Green dots materialize the position of the aSyn inclusions in the sections (Lewy neurites, NCIs, NIIs, GCIs and GNIs). Note the strikingly analogous anatomical spread patterns in the 1B and MSA conditions and the absence of pathology in the « M83-only » condition. Scale bar = 3 mm.*

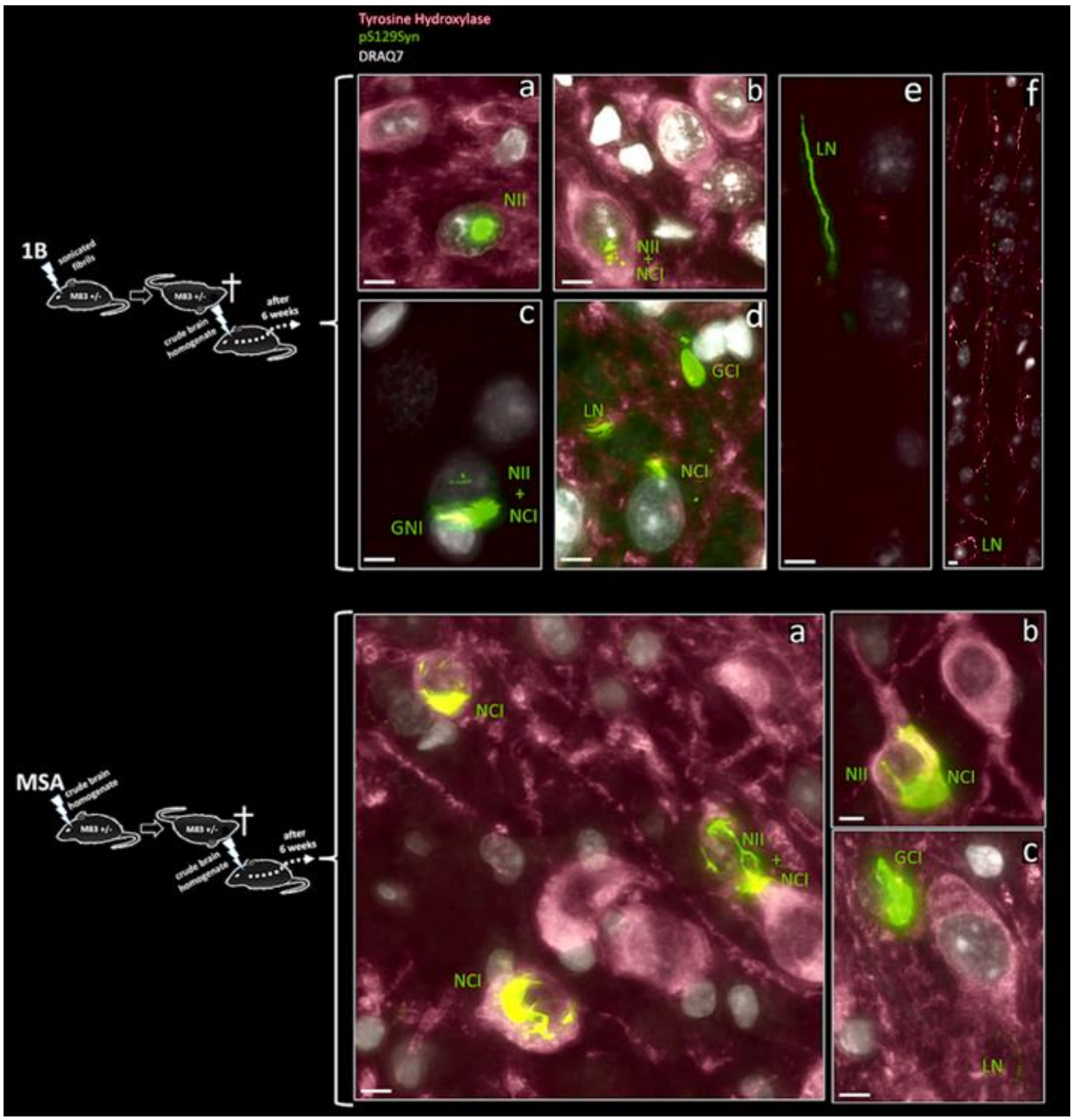

Color-blind version of Extended Data Fig. 6 *(generated using the software Visolve Deflector 4.5)* | ***animal-to-animal transmission of aSyn pathology. 1B transmission panels:*** *examples of aSyn inclusions detected 6 weeks after crude brain homogenate inoculation in a wild-type mouse. NII: neuronal intranuclear inclusion; NCI: neuronal cytoplasmic inclusion; GNI: glial nuclear inclusion; LN: Lewy neurite; GCI: glial cytoplasmic inclusion.* ***a, b, d*** *are from the right SNpc,* ***c, e*** *and* ***f*** *are from cortical regions.* ***MSA transmission panels:*** *examples of aSyn inclusions detected 6 weeks after crude brain homogenate inoculation in a wild-type mouse. Abbreviations are the same as in before.* ***a, b*** *and* ***c*** *are from the right SNpc. Scale bars = 5 µm. See corresponding 3D reconstructions and animations in Supplementary materials.*

Tables

Table 1: Cryo-EM data collection, refinement, and validation statistics

1B aSyn fibrils Raw images: EMPIAR-12012 Reconstructed volume: EMD-19986 Atomic model: PDB-9EUU	
Data collection and processing	
Nominal Magnification	120’000x
Voltage (kV)	300
Total electron dose (e/Å^2)	40
Defocus range (μm)	-0.8 to -1.8
Pixel size (Å)	0.66
Symmetry imposed	C1 with 2_1 cork-screw symmetry
Micrographs	11’879
Initial particle images (no.)	108’543
Final particle images (no.)	51’272
Map resolution (Å) FSC threshold at 0.143	 1.94
Map resolution range (Å)	1.88-2.56
Estimated map sharpening B-factor (Å^2)	-21.06
Helical twist (°)	179.52
Helical rise (Å)	2.43
Refinement	
Model resolution range (Å)	1.7 - 2.4
Model composition Non-hydrogen atoms Protein residues Ligands	 3400 496 0
B factor (Å^2) Protein	 21.06
R.m.s. deviations Bond lengths (Å) Bond angles (°)	 0.001 0.490
Validation MolProbity score Clashscore Poor rotamers (%)	 1.52 5.57 0.00
Ramachandran plot Favored (%) Allowed (%) Disallowed (%)	 96.61 3.39 0.00